Estuarine, Coastal and Shelf Science 306 (2024) 108897

Contents lists available at ScienceDirect

Estuarine, Coastal and Shelf Science

journal homepage: www.elsevier.com/locate/ecss

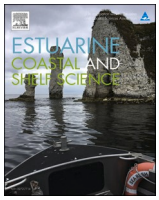

CDOM dynamics in two coastal zones influenced by contrasting land uses in northern Patagonia

Elizabeth D. Curra-Sánchez [a,b,c,*], Aline de M. Valerio [d,e], Carlos Lara [f,g], Wirmer García-Tuñon [h,i], Bernardo R. Broitman [c,j], Gonzalo S. Saldías [c,k], Jorge Nimptsch [l], Cristian A. Vargas [b,c]

[a] Facultad de Ingeniería y Negocios, Universidad de Las Américas, Sede Concepción, Concepción, Chile
[b] Laboratorio de Ecosistemas Costeros y Cambio Ambiental Global (ECCALab), Departamento de Sistemas Acuáticos, Facultad de Ciencias Ambientales y Centro de Ciencias Ambientales EULA Chile, Universidad de Concepción, Concepción, Chile
[c] Instituto Milenio en Socio-Ecología Costera (SECOS), Pontificia Universidad Católica de Chile, Santiago, Chile
[d] Monitoring Ocean from Space Laboratory (MOceanS), National Institute for Space Research (INPE), São José dos Campos, São Paulo, Brazil
[e] Center for Nuclear Energy in Agriculture (CENA), University of São Paulo, Piracicaba, São Paulo, Brazil
[f] Departamento de Ecología, Facultad de Ciencias, Universidad Católica de la Santísima Concepción, Concepción, Chile
[g] Centro de Investigación en Recursos Naturales y Sustentabilidad, Universidad Bernardo O'Higgins, Santiago, Chile
[h] Data Observatory Foundation, ANID Technology Center No. DO210001, Chile
[i] Programa de Doctorado en Ciencias con Mención en Biodiversidad y Biorecursos, Facultad de Ciencias, Universidad Católica de la Santísima Concepción, Concepción, Chile
[j] Departamento de Ciencias, Facultad de Artes Liberales, Universidad Adolfo Ibáñez, Viña del Mar, Chile
[k] Departamento de Física, Facultad de Ciencias, Universidad del Bío-Bío, Concepción, Chile
[l] Instituto de Ciencias Marinas y Limnológicas, Laboratorio de Bioensayos y Limnología Aplicada, Facultad de Ciencias, Universidad Austral de Chile, Valdivia, Chile

ARTICLE INFO

Keywords:
Land use change
CDOM
Interannual variability
Northern Patagonia
Landsat

ABSTRACT

Colored dissolved organic matter (CDOM) is an indicator and optical proxy of terrestrial processes such as land use with allochthonous material fluxes, biogeochemical cycles, and water quality in coastal zones influenced by rivers. However, the role of land use changes on the spatial and temporal availability of CDOM has been poorly explored in Chile. Here, we studied two watersheds with similar climates and contrasting land use patterns in northern Patagonia considering the sampling of CDOM in their estuarine and adjacent coastal ocean. An empirical algorithm with the coefficients adjusted to our study areas to estimate CDOM was applied to Landsat 7 and 8 images to examine temporal variability of CDOM*est* from 2001 to 2011 and 2013–2020. Our results showed an increasing trend of CDOM*est* in both areas. Different trends in land use patterns between the two watersheds showed a significant correlation with CDOM*est* and contrasting associations with environmental variables. Higher humification was found in Yaldad in comparison with Colu. In both areas, allochthonous materials predominated, especially during austral spring according to the low values of the Fluorescence Index (FI). Our results highlight the potential of CDOM*est* to parameterize biogeochemical cycling models and to further understand the dynamics of CDOM in coastal ecosystems.

1. Introduction

Colored dissolved organic matter (CDOM), commonly known as gelbstoff or yellow substance, is the fraction of aquatic dissolved organic matter that absorbs radiation from ultraviolet to near-infrared wavelengths (Zhao et al., 2018; Bricaud et al., 1981). CDOM is ubiquitous in aquatic ecosystems and constitutes a complex mixture of substances, including humic and fulvic acids (Pandi et al., 2021; Zhang et al., 2021; Fellman et al., 2010; Coble, 2007). Humic acid-like compounds are more commonly associated with a terrestrial origin and have a higher molecular weight than fulvic acids, which are more degraded (He et al., 2021; Fellman et al., 2010; Coble, 2007). To date, most of the literature emphasizes that the processes influencing the generation, transport, and transformation of CDOM impact the biogeochemical cycles of water

* Corresponding author. Facultad de Ingeniería y Negocios, Universidad de Las Américas, Sede Concepción, Concepción, Chile.
E-mail address: elicurra@udec.cl (E.D. Curra-Sánchez).

https://doi.org/10.1016/j.ecss.2024.108897
Received 26 April 2024; Received in revised form 3 July 2024; Accepted 29 July 2024
Available online 31 July 2024

bodies, chiefly in photochemically-mediated processes of the water column (Hu et al., 2017; Zhang et al., 2009). Different studies have shown that CDOM in coastal waters comes from i) allochthonous sources, which mostly include degraded organic matter from the surrounding terrestrial environment, which is typically exported via river discharges or sewage into the coastal ocean (Valerio et al., 2021; Ward et al., 2017; Coble, 2007), and ii) autochthonous sources, which include the remains of phytoplankton, macrophytes, and bacteria (Roiha et al., 2016; Zhang et al., 2009, 2013). Studies have also outlined that photochemical and microbial processes are important for CDOM degradation (Fasching et al., 2014; Lapierre et al., 2013). By transforming complex molecules into more labile materials (e.g., proteins-like), degraded CDOM can be further utilized by phytoplankton and microorganisms (Grunert et al., 2021; Fasching et al., 2014; Lapierre et al., 2013).

CDOM has been extensively studied using *in situ* measurements and spectrophotometric and spectrofluorometric techniques. Some investigations have used absorption coefficient at specific wavelengths (aCDOM(λ)), the slope of the CDOM absorption curve (S) and indices (e.g., fluorescence and humification index) to study the magnitude (Pandi et al., 2021; Helms et al., 2008) and to distinguish the different origins and degree of CDOM transformation (Fellman et al., 2010; Huguet et al., 2009; McKnight et al., 2001). Recently, *in situ* measurements in combination with satellite estimates (CDOM*est*, e.g. Drozdova et al., 2021; Valerio et al., 2021) can be used to monitor CDOM as a proxy indicator of the export of terrestrial materials to the coastal ocean (Nezlin et al., 2020; Osburn et al., 2016; Slonecker et al., 2016; Kutser et al., 2015). Studies highlight the importance of land-ocean interactions, which are not only affected by climate change (Boyd et al., 2015; Regnier et al., 2013) but also by anthropogenic activities (e.g., land cover change; Chen et al., 2021; Wang and Zhang, 2018; Wilson and Xenopoulos, 2009). These activities occur at a global scale, with impacts on the biogeochemistry of aquatic ecosystems (Ward et al., 2017; Roiha et al., 2016; Nelson and Siegel, 2013).

In Chile, there are two important economic activities that are growing exponentially: aquaculture (i.e.: mithilid and salmon farming, FAO, 2020) and agriculture together with forestry plantations (*Pinus* and *Eucalyptus* spp., Alvarez-Garreton et al., 2019). Although these activities influence the nearby ecosystems, changes in land use can have a short-to medium-term impact on aquaculture (Nimptsch et al., 2015; Pérez et al., 2015; Silva et al., 2011). This is because they can modify the physical and chemical properties of the soil as well as the composition and amount of organic matter that flows into water bodies, increasing turbidity, nutrient inputs, changing biogeochemical cycles, and among other (Curra-Sánchez et al., 2022; León-Muñoz et al., 2021; Pérez et al., 2015). Land uses and land use changes in river basins can influence the amount and composition of organic and inorganic matter exported into the coastal ocean (Razali et al., 2018; Graeber et al., 2015; Pérez et al., 2015, Shao and Wang, 2020). Several studies suggest a relationship between terrestrial inputs and the quality of CDOM, differentiating between natural (e.g., forests, wetlands) and anthropogenic (e.g., urban, agricultural) inputs (Lambert et al., 2017; Fellman et al., 2010; Wilson and Xenopoulos, 2009). The potential effects of CDOM on ocean color and biogeochemistry have been previously described (e.g., Sánchez-Pérez et al., 2020; Hu et al., 2017; Coble, 2007). However, the estimation and distribution of CDOM across estuarine and coastal waters remains challenging due to the influence of multiple environmental factors and high temporal variability along the land-ocean interface (Zhang et al., 2021; Zhao et al., 2018). In Chile, and especially in northern Patagonia where these anthropogenic activities converge, there are very few studies on their impacts and on the use of CDOM as a nexus of terrestrial influence (e.g., Curra-Sánchez et al., 2022; González et al., 2019; Nimptsch et al., 2015). In the present study, we evaluated the relationship of CDOM with different land uses. For this, we compared two remote and sparsely observed watersheds and their adjacent coastal zones in northern Patagonia, Chile. Thus, we aim to analyze the influence of land use changes on the availability of CDOM in the river-influenced coastal zones. Considering the application and relationship of different parameters obtained by optical and fluorescence spectroscopy to evaluate the dynamics of CDOM in the contrasting study areas, together with the application of empirical algorithms associated with remote sensing, our analyses provide a better understanding of the relationship of land use with CDOM in the studied water bodies.

2. Materials and methods

2.1. Study area

The study region includes the adjacent coastal ocean of two watersheds with contrasting land uses in Chiloé Island, Chile (Fig. 1). The Colu River basin has an area of 77.31 km^2 (Fig. 1b) and has been extensively modified by anthropogenic intervention (Curra-Sánchez et al., 2022). The Yaldad River basin has an area of 271.06 km^2 (Fig. 1c) and is dominated by native forest within a large protected area (Biblioteca del Congreso Nacional de Chile, www.bcn.cl and Dirección General de Aguas, www.dga.cl). Both basins are characterized by freshwater flowing towards the Inner Sea of Chiloé (ISC). The climate is temperate maritime, with a mean annual temperature of 11 °C and year-round rainfall (between 2000 and 4000 mm) with seasonality of higher precipitation during fall and austral winter, and extensive cloud cover (Lara et al., 2018; Subiabre and Rojas, 1994). The bathymetry in the coastal zones is relatively shallow, reaching maximum depths of ~140 m. The tidal amplitude is ~5 m, with a semi-diurnal regime throughout the year (Clasing et al., 1994). Surface salinity fluctuates between 29 and 32 PSU at Colu and 26 to 33 PSU at Yaldad, with lower values at the river mouth (Curra-Sánchez et al., 2022). Sea surface temperature fluctuates between 10-12.5 °C and 13–14.6 °C in Colu and Yaldad, respectively (Curra-Sánchez et al., 2022; Clasing et al., 1994). In general, the main economic activities on the Island and Inner Sea of Chiloe are fishing and agriculture, together with the aquaculture of mussel and salmon (FAO, 2020; SERNAPESCA - Servicio Nacional de Pesca y Acuicultura, 2018). In the study areas, mussel aquaculture is developed in Yaldad Bay and salmon farming in the areas near the coastal zone of Colu (SERNAPESCA - Servicio Nacional de Pesca y Acuicultura, 2018).

2.2. In situ data collection

We collected data during two sampling campaigns in January and November 2019 (austral summer and spring, respectively) [Supplementary Material (SM), Table S1]. Samples were collected for 2 day at each of the 8 sampling stations for summer (16) and spring (16) in both study areas (Colu and Yaldad) with a total of 64 samples. Surface water samples for CDOM and Fluorescent Dissolved Organic Matter (*f*DOM) components were collected during the morning at low tide, along six stations distributed in the adjacent coastal, and two stations in the riverine-estuarine area of each study site (Colu coastal zone and in Yaldad Bay) (Fig. 1b and c). *In situ* and simultaneous salinity (PSU) and temperature (^{o}C) profiles were collected using a CTD (SEA-BIRD 19plus V2 SeaCAT Profiler).

Surface samples for CDOM analyses were collected and filtered by swinex with 0.2 μm polyethersulfone membrane filters (Millex-GP Millipore-Express (PES), sterile), previously conditioned in the field with 100 mL of chromatographic water or ultra-pure water in triplicate and stored in 40 mL amber vials, previously acid washed (HCl 10%) and pre-combusted for 7–8 h at 480 °C. Samples were stored (maximum 72 h) at a temperature of 4 °C until their analysis in the Laboratory of Applied Limnology, Instituto de Ciencias Marinas y Limnologicas, Facultad de Ciencias, Universidad Austral de Chile, Valdivia, Chile (Nimptsch et al., 2014, 2015). CDOM absorption coefficient (aCDOM (λ)) was calculated from absorbance measurements using the following equation:

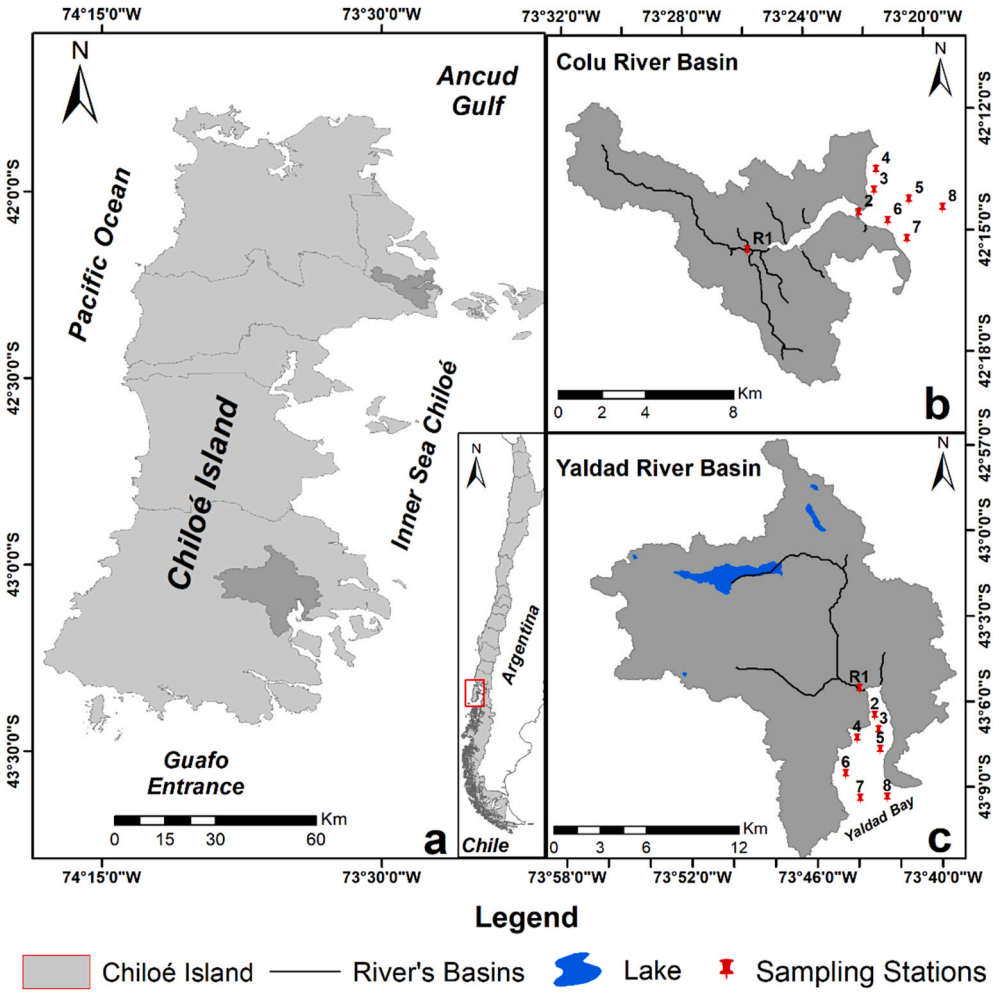

Fig. 1. (a) Study area in Chiloé Island, northern Patagonia, Chile. Sampling stations for *in situ* CDOM analysis in water samples are shown in red in (b) and (c). (For interpretation of the references to color in this figure legend, the reader is referred to the Web version of this article.)

$$aCDOM\ (\lambda) = 2.303*A(\lambda) / L \quad (1)$$

where A(λ) is the absorbance of the filtered seawater sample at the specific wavelength λ and L is the optical pathway of the quartz cell (5 cm). The absorbance of aCDOM (λ) was determined by a CADAS200 UV/VIS spectrum of absorbance (Dr. Lange, Germany) within a wavelength range 190–800 nm and corrected for internal backscatter measured at 700 nm (Bricaud et al., 1981). The absorption coefficient was measured at room temperature (25 °C). This measurement was converted to CDOM absorption coefficient (m^{-1}) according to the methodology proposed by the American Public Health Association (APHA, 2005; Bricaud et al., 1981). The absorption coefficient of 440 nm (aCDOM (440)) was used in this study to describe the amount of CDOM in the water and as a wavelength complement for use in remote sensing (Miller, 1981). The fraction of CDOM that emits radiation such as fluorescence is called Fluorescent Dissolved Organic Matter (*f*DOM) and its composition was determined by fluorescence spectroscopy with an Agilent Cary Eclipse fluorescence spectrophotometer and expressed in Raman units (R.U) (Lawaetz and Stedmon, 2009). The size of the cuvettes used for the measurements was 1 cm for *f*DOM (R.U) and 5 cm for aCDOM (m^{-1}) components. Fluorescence was taken at excitation wavelengths from 240 to 450 nm (5 nm steps) and emission wavelengths from 300 to 600 nm (2 nm steps) with a slit width of 5 nm. The composition and potential sources of CDOM and *f*DOM were estimated using a Parallel Factor Analysis Model (PARAFAC). The PARAFAC analysis identified five components (SM Table S2). These five components were classified according to Coble et al. (1998) and Fellman et al. (2010): humic acids UVC (H.A UVC), humic acids UVA (H.A UVA), fulvic acids (F.A), protein-like and tyrosine. These components were validated in halves (SM Figs. S1 and S2), and the best fit of the model was established by random initialization (Stedmon and Bro, 2008).

From the absorption coefficient spectra of CDOM in the UV domain, spectral slope indices were calculated for 275–295 nm (S275-295), 350–400 nm (S350-400) and the ratio of the two slopes (SR = S275-295/S350-400). Spectral slopes provide information on the composition, origin, molecular weight, and bioavailability of CDOM (Fichot and Benner, 2012; Helms et al., 2008). Higher S275-295 values are often associated with increased photochemical degradation of DOM (Zhang et al., 2009; Helms et al., 2008). While lower values of S275-295 and SR are related to compounds of higher molecular weight and lower degradation (e.g., Valerio et al., 2018; Vantrepotte et al., 2015; Nelson and Siegel, 2013; Romera-Castillo et al., 2013; Helms et al., 2008).

We used two indices to distinguish the different origins and the degree of transformation of CDOM in this study. First, the fluorescence index (FI), calculated as the ratio between the intensities 450/500 for an excitation wavelength of 370 nm (McKnight et al., 2001). Second, the humification index (HIX), calculated as the ratio between the fluorescence emission spectra (300 and 480 nm) and an excitation wavelength of 254 nm (Huguet et al., 2009). Fluorescence index allowed the characterization of the CDOM source. Its values ranged from 0 to 2. High FI values (greater 1.8) generally indicate an autochthonous and microbial fluorescence character, while a low FI (1.4) suggests an allochthonous

and terrestrial fluorescence character. Intermediate FI values are found in CDOM waters from mixed sources (Shafiquzzaman et al., 2020; Cawley et al., 2012). The humification index (HIX) estimates the degree of transformation of organic matter in the water (Huguet et al., 2009). There is no universal set of reference values for the HIX index in the scientific community, as these may vary according to the type of sample and environmental conditions. However, a consensus has been reached that a higher HIX value indicates a higher degree of humification with organic matter that has been transformed or aged. In contrast, a lower value indicates a higher proportion of fresh or less transformed organic matter (Shang et al., 2019; Chen et al., 2011).

2.3. Image collection and processing

40 satellite images from Landsat 7 and 8 were used for both study areas (Colu coastal zone and Yaldad Bay). A period of 18 years (2001–2011 and 2013–2020) was used in the analysis of CDOM, whereas 20 years (2000–2020) covered the analysis of land use change. Satellite images for the years 2000 and 2012 were not considered due to the high percentage of cloud cover. For both sites (Path: 233 and Rows: 89 Colu/90 Yaldad), we used satellite images for austral summer as cloud-free images were not available during other seasons (SM Table S3). The main criteria for selecting the working images were 0% cloud cover and satellite images on the same dates for both areas. Based on these criteria, satellite images from Landsat 7 (ETM+) and 8 (OLI/TIRS) (Landsat Collection 1 Level-1 dataset) with a spatial resolution of 30 m were obtained from the USGS Earth Explorer website (https://earthexplorer.usgs.gov/) (USGS Earth Explorer, n.d.) for the CDOM*est* and land use change analyses. Following the high cloud cover of the study area, the requirement of a close temporal match-up between satellite and *in situ* data, and the coarse temporal resolution of Landsat images (periodicity of 16 days), we winnowed satellite data to one image per period (year). Hence, our backwards reconstruction of CDOM*est* was restricted to the austral summer, thus limiting our conclusions, yet providing a more reliable interpretation of our results.

The Landsat images were acquired as Level-1 data, consisting of quantized and calibrated scaled digital number (DN) values. To convert these to water leaving reflectance (ρ), the following steps were considered: (i) Obtaining absolute Top-Of-Atmosphere (TOA) reflectance (ρ_p) from scaled DN values (Equations (2) and (3)), and (ii) Converting TOA reflectance to water leaving reflectance (Equation (4)). For this process, we used the open-source software QGIS 3.16 (OSGeo Foundation) using the Semi-Automatic Classification Plugin (SCP version 7.1) (Congedo, 2021).

$$L_\lambda = M_L * Q_{cal} + A_L \quad (2)$$

where: M_L is Band-specific multiplicative rescaling factor from Landsat metadata; Q_{cal} is Quantized and calibrated standard product pixel values (DN) and; A_L is Band-specific additive rescaling factor from Landsat metadata.

$$\rho_p = [\pi * L_\lambda * d^2] / (ESUN_\lambda * \cos\theta_s) \quad (3)$$

where: L_λ = Spectral radiance at the sensor's aperture; d = Earth-Sun distance in astronomical units; $ESUN_\lambda$ = Mean solar exo-atmospheric irradiances; θ_s = Solar zenith angle in degrees, which is equal to θ_s = 90° - θ_e where θ_e is the Sun elevation.

$$\rho = [\pi * (L_\lambda - L_p) * d^2] / T_v((ESUN_\lambda * \cos\theta_s * T_z) + E_d) \quad (4)$$

where: L_p is the path radiance; T_v is the atmospheric transmittance in the viewing direction; T_z is the atmospheric transmittance in the illumination direction; E_d is the downwelling diffuse irradiance.

More information is available in the SCP plugin manual, and it is further supplemented by Section 1.1 of our Supplementary Material.

Data of sea surface temperature (SST, °C), chlorophyll-a (Chl*a*, mg m^{-3}), instantaneous photosynthetically active radiation (iPAR, Einstein m^{-2} s^{-1}) and normalized fluorescence line height (nFLH, mW cm^{-2} μm^{-1} sr^{-1}) for the Inner Sea of Chiloé (ISC) were obtained from MODIS onboard the Aqua satellite (MODIS-A) with a spatial resolution of 1 km and over a time window of 17 years. L1A images from MODIS-A (Moderate Resolution Imaging Spectroradiometer) were obtained from the NASA Ocean Color (https://oceancolor.gsfc.nasa.gov/) and MODIS portals (https://modis.gsfc.nasa.gov/data/dataprod/). The processing was carried out according to Behrenfeld et al. (2009), and Saldías and Lara (2020). We restricted the dataset to information available only for dates coinciding with CDOM*est*. Precipitation data (Pp, mm) for the entire temporal analysis were obtained from weather stations located in the study areas and visualized using the Climate Explorer (www.cr2.cl), an online tool for visualizing public climate data developed by the Climate Science and Resilience Center (CR2) and implemented by Meteodata (CR2, 2021). We selected data corresponding with the precipitation accumulated over the month prior to the one in which the satellite CDOM data were extracted. This, with the purpose of assessing the effect of precipitation on the transport of organic matter to the coastal zone. General information on the dates and sensor of image acquisition can be reviewed in the supplementary material (SM Table S3).

2.3.1. Satellite CDOM estimation

For the CDOM estimation (CDOM*est*) we utilized a total of 36 Landsat images for both study areas (18 for Colu coastal zone and 18 for Yaldad Bay) and used one image per year to represent the austral summer. The temporal analysis was performed for a period of 18 years (2001–2011 and 2013–2020), using one month of austral summer per studied year (SM Table S3).

We tested several empirical algorithms (e.g., Chen et al., 2017; del Castillo and Miller, 2008; D'Sa and Miller, 2003; Ficek et al., 2011; Kutser et al., 2015; Mannino et al., 2014; Slonecker et al., 2016; Tiwari and Shanmugam, 2011) with different band relationships (SM Table S4), considering the conditions of the area. Since the tested empirical algorithms implemented band ratios, water leaving reflectance (ρ) was used, as it considers the relative values between bands rather than the absolute value of the physical parameter. This information is supplemented by Table S4 and Section 1.2 of the Supplementary Material. The *in situ* CDOM data and the selected bands were used to obtain the coefficients (SM Table S5), adjusted for the study areas (Colu and Yaldad) during the sampling campaigns in summer and spring. Empirical algorithms (SM Fig. S3, Table S6) were constructed using these adjusted coefficients. Considering the availability of images and cloud cover in both areas, the time series was constructed for the austral summer. The summer algorithms for Colu (Equation (5)) and Yaldad (Equation (6)) are shown below:

$$CDOM443 = 0.1157 * \rho(412) \Big/ \rho(555)^{-8.533} \quad (5)$$

$$CDOM443 = 0.3155 * \rho(412) \Big/ \rho(555)^{-9.283} \quad (6)$$

These new empirical algorithms (SM, Table S6) were used to create the CDOM time series for both study areas.

2.3.2. Land uses classification from satellite images

The land use and land use changes (LULUC) for the study areas were identified from Landsat data collection for the years 2000, 2005, 2010, 2014, and 2020. The analysis and quantification of the most significant land cover changes comprised a 20-year period, then we compared the periods 2000–2005, 2000–2010, 2000–2014, and 2000–2020. The LULUC classification was made based on six straightforward land cover types (1) native forest, (2) shrubland, (3) bare soil, (4) grassland-agriculture (includes crop rotations, agriculture, livestock), (5) water bodies (rivers, lakes, and lagoons) and (6) wetlands. These categories

were simplified and adapted from the "General Vegetation Classification System developed for the project "Inventario y evaluación de los recursos vegetales autóctonos de Chile" (Corporación Nacional Forestal/Universidad Austral de Chile, 2014).

The supervised classification method was used to identify the different land uses in the satellite images. This method consisted of selecting representative areas for each land use (Hao et al., 2021; Chen et al., 2020). For the construction of the spectral signature, we select the Maximum Likelihood statistical criterion (Chuvieco, 2010; Aguayo et al., 2009), to classify the images according to the categories defined above. The classification was supported by the Confusion Matrix, which evaluates the accuracy of the classification using the Kappa Coefficient (>0.96) and Overall Accuracy (95–99%) indicators. The closer they rank to 1 and 100%, respectively, the better (Chuvieco, 2010). The above analysis was complemented with three sources of information: the cartographic database of the Inventory and Evaluation of Native Plant Resources of Chile (Corporación Nacional Forestal/Universidad Austral de Chile, 2014), high-resolution images available in Google Earth (http://earth.google.com), and 99 control points taken in the field with GPS for those coverages that presented greater confusion (Hao et al., 2021; Aguayo et al., 2009). The land cover change was quantified using a transition matrix consisting of a symmetrical double-entry table indicating land cover and in each cell the surface of the areas that changed between 2000 and 2020. The transition matrix was constructed from the superposition and map algebra (Hao et al., 2021; Aguayo et al., 2009).

The rate of change (r) was calculated using the following formula:

$$r = (S2/S1)^{\left(\frac{1}{t2-t1}\right)} - 1 \quad (7)$$

where t1 and S1 are the initial time and surface area, while t2 and S2 are the final time and surfaces, respectively (Aguayo et al., 2009; FAO, 1996).

2.4. Statistical analyses

To normalize the data and compare all the variables, we used standardized anomalies (Ogallo and Gbeckor-Kove, 1989). A *t*-test was applied to check if there were differences between both study areas (Colu coastal zone and Yaldad Bay) in terms of CDOM*est*, precipitation, SST, Chl*a*, iPAR, nFLH. A *t*-test was also applied to observe differences between study areas and campaigns (summer and spring) for the following parameters: CDOM, spectral slopes (S275–295, S350-400), ratio of the two slopes (SR = S275-295/S350-400), fluorescence index and humification index. We also examined the correlation between all the variables using Spearman's rank correlation (R_s) for each of the study zones. The variables (CDOM, *f*DOM components, salinity) were normalized and a two-way Anova test was applied to evaluate if there were significant differences between zones and campaigns. The Mann-Kendall trend test is used to analyze the significance of the increasing or decreasing trend of the data collected over time. To synthesize the multivariate relationships between environmental parameters and land use patterns in both river basins, we performed a principal component analysis (PCA). Data management and analysis was carried out using the software OriginPro 2021b Student Version. The analyses can be reviewed in the Supplementary Material (SM).

3. Results

3.1. CDOM/fDOM quality

The highest CDOM values were recorded in both rivers (1.41–5.33 m^{-1}), being significantly higher in Yaldad during all campaigns (SM Table S1, Fig. S4). CDOM was significantly higher during spring in both zones (ANOVA two-way, Factor = 'zone', df = 1, F = 9.512, p = 0.003 and Factor = 'Campaign', df = 1, F = 7.098, p = 0.010; SM Table S8). The protein-like compound was higher in the coastal stations of Colu than in Yaldad (ANOVA two-way, Factor = 'Campaign', df = 1, F = 24.844, p < 0.001; interaction between Factor = 'campaign' and 'zone', df = 1, F = 6.343, p = 0.015, SM Table S8). On the other hand, for the tyrosine-like compound, no significant differences were observed between zones but between campaigns (ANOVA two-way, Factor = 'Campaign', df = 1, F = 7.019, p = 0.010; SM Table S8). While the rest of the *f*DOM components (SM Fig. S4, UVC humic acids, UVA humic acids, fulvic acids) were significantly higher in Yaldad than in Colu (SM Table S1, Table S8, Fig. S4). The decreasing behavior of CDOM and *f*DOM components from the river towards the coastal stations (SM Fig. S4) coincides with the increase in salinity in the same direction (SM Table S1, Fig. S5).

The S275-295 and SR ratio between S275–295 and S300-350 presented higher values in the coastal zone of Colu (Table 1). These results showed that *in situ* CDOM at Colu had lower molecular weight or was potentially more photo-degraded during its transport to the coastal ocean. On the other hand, the low values for spectral slopes in Yaldad Bay suggested that *in situ* CDOM had a higher molecular weight (higher lignin, fulvic and humic acid content), and was less degraded (Wagner et al., 2015; Fichot and Benner, 2012; Helms et al., 2008). It also corresponds with the CDOM/*f*DOM results, where the highest values are observed at both rivers (SM Table S9, Fig. S4).

The FI showed significant differences between zones (t_test, $p < 0.001$; SM Table S10) and study campaigns (t_test, $p < 0.01$, SM Table S11). The highest value (FI = 3.52) was observed during the austral summer in Colu. Stations 1 (Colu River station) and 4 are the exception because terrestrial material predominated (Fig. 2, SM Table S10). On the other hand, terrestrial material predominated throughout the stations, except in station eight (FI = 1.64), where the FI value determined that the source was of microbial origin in Yaldad. However, during the spring campaign in both areas the FI indicated a source derived from terrestrial materials (FI: 0.57–1.5) (Fig. 2, SM Table S10).

Fig. 2 shows the values of the FI and HIX indices for each of the sampling seasons. A gradient can be observed from the river towards the stations with greater marine influence as the HIX decreased seaward (Fig. 2, SM Table S9). The highest values were recorded in the river station of both zones during the two campaigns (Colu: 2.40 and 6.22; Yaldad: 6.01 and 9.04, summer and spring, respectively) and decreased towards the stations with greater marine influence (Fig. 2, SM Table S9). This pattern matches the CDOM data observed for both zones and is consistent with the significant positive correlation between HIX and CDOM (R_s) = 0.86, $p \leq 0.001$, SM Fig. S6). This strong relationship is also observed (SM Fig. S6) between Slope 275–295 and HIX but negatively ($R_s = -0.87$, $p \leq 0.001$) However, the relationship between Slope 275–295 and FI is positive but weak ($R_s = 0.38$, $p \leq 0.05$).

3.2. Environmental variables and their relationship with CDOMest

The match-up of the summer algorithms applied to the time series showed a regression with a significantly high coefficient of determination (R2 >0.5) and lower root mean square deviation (RMSE ≤0.1) for both zones (SM Fig S3 a, b and Table S7) despite being few points (8). Mean Bias Error (MBE) showed an underestimation of the model in Colu and an overestimation in Yaldad (SM Fig. S3 a, b), during the austral

Table 1
Spectral parameters (Slope value of 275–295, Slope value of 350–400) and slope ratio (SR) measured for each area in 2019.

Zone	With river data			Without river data		
	S275-295 (nm)	S350-400 (nm)	SR (nm)	S275-295 (nm)	S350-400 (nm)	SR (nm)
Colu	0.016	0.017	0.96	0.021	0.017	1.217
Yaldad	0.014	0.015	0.905	0.014	0.014	1.05

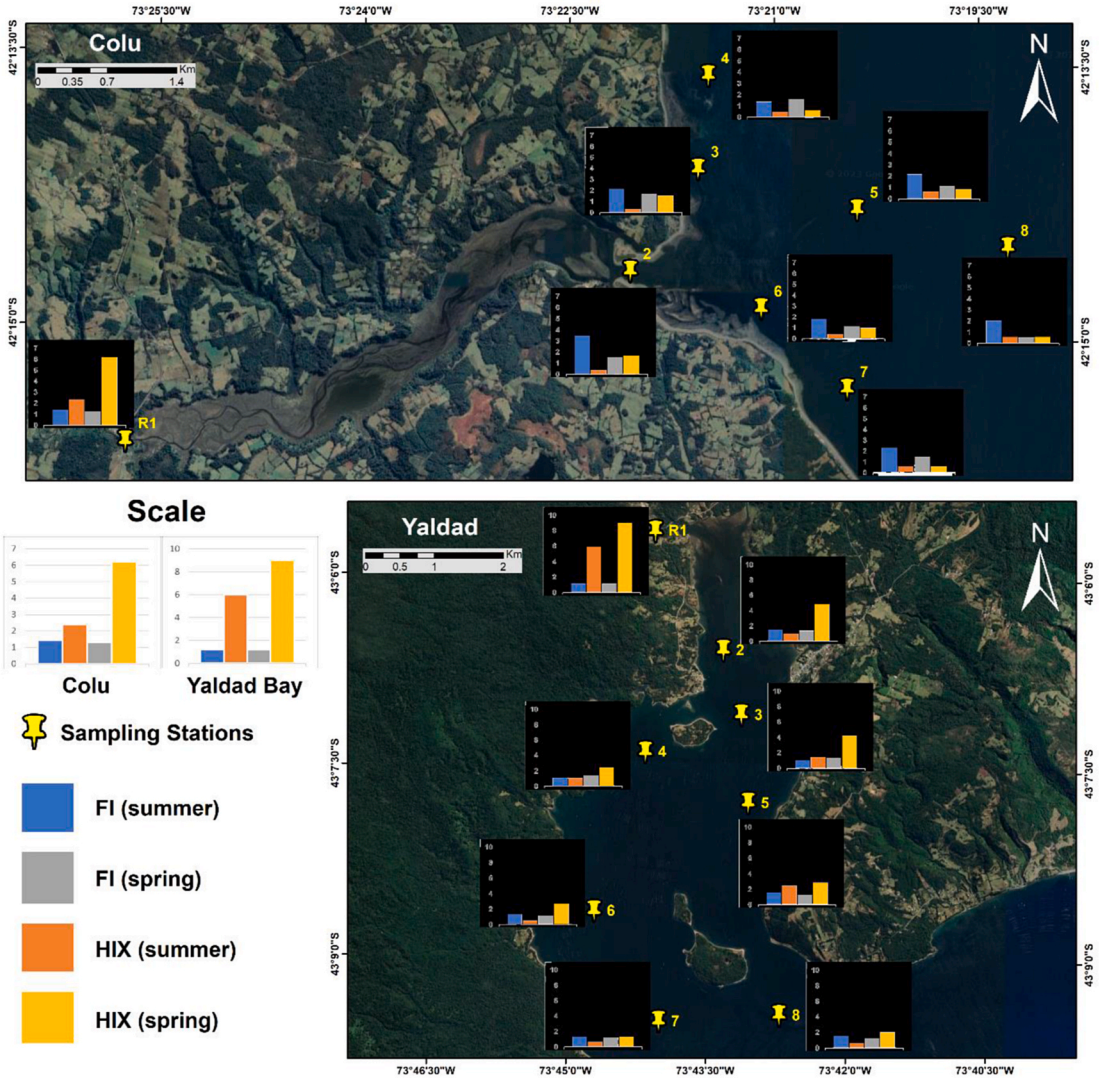

Fig. 2. Average Fluorescence (FI) and Humification (HIX) indices by study area (Colu and Yaldad), sampling campaign, and by season (summer and austral spring). The colors represent the values of FI and HIX for summer and spring. (For interpretation of the references to color in this figure legend, the reader is referred to the Web version of this article.)

summer. While during the spring the opposite occurred (SM Fig. S3 c, d). However, for both campaigns the overestimation and underestimation were of small magnitudes.

Considering the above and that the summer images showed less cloudiness, the temporal analysis was applied to the austral summer data for both areas. Therefore, the time series was constructed only for summer with the Colu Summer (CS) and Yaldad Summer (YS) algorithms (SM Table S6).

The spatial distribution of CDOM*est* for the year 2019 is shown in Fig. 3. The maximum CDOM*est* values for each study area were concentrated at the river mouths and along the coast (runoff). The lowest CDOM*est* values (dark blue) were observed in seawater or areas with marine influence. The distribution of the colors indicating the ranges of CDOM values show the spatial distribution and influence of freshwater and seawater in the study areas.

The CDOM*est* (Fig. 4a, SM Table S12) showed low values (0.004–0.01 m^{-1}) from 2001 to 2006 in both. However, it increased during 2007 and stayed high until the end of the time series in 2020 (0.115–0.946 m^{-1}), with slight fluctuations in certain periods. The exception to this incremental pattern after 2007 was the years 2008, 2010 and 2015 when low CDOM*est* was observed (SM Table S12), but more significant in Yaldad (0.461 m^{-1} and 0.619 m^{-1}). The highest CDOM*est* value was observed in 2007 and 2013 for the area of Colu (0.194 m^{-1}) and Yaldad (0.946 m^{-1}), respectively. The CDOM*est* values showed significant differences between study areas (*t*-test, $p < 0.0001$, SM Table S13). We observed clear differences between the study zones starting in 2007 and during the years 2013, 2014 and 2020 (Fig. 4, SM Table S12), and therefore, other parameters such as land use change (sections 3.3) were analyzed to examine their relationships with CDOM*est*.

From the standardized anomalies an increasing trend is observed for CDOM*est* and iPAR (Fig. 4a–e), although only CDOM*est* had a significant trend according to the Mann-Kendall test (SM Table S14). On the other hand, Pp, SST and Chl*a* presented a slightly decreasing trend (Fig. 4b, c, d). In contrast, nFLH seemed to decrease slightly in Yaldad Bay and increase in the coastal zone of Colu (Fig. 4f). The Mann-Kendall test only showed significant trends for SST and Pp in Yaldad (SM Table S14).

Significant differences in SST, Chl*a* (*t*-test, $p < 0.0001$; SM Table S13) and nFLH (*t*-test, $p = 0.018$, SM Table S13) were observed between both zones. The highest values of precipitation (7.355 mm), SST (15.3 °C), Chl*a* (32.7 mg m^{-3}), iPAR (59.6 E m^{-2} s^{-1}) and nFLH (0.59 mW cm^{-2} μm^{-1} sr^{-1}) were observed in the Colu zone (Fig. 4; SM Table S10). Moreover, the minimum values of all were observed in Yaldad zone, except for nFLH and CDOM*est*, where the minimum was recorded in the

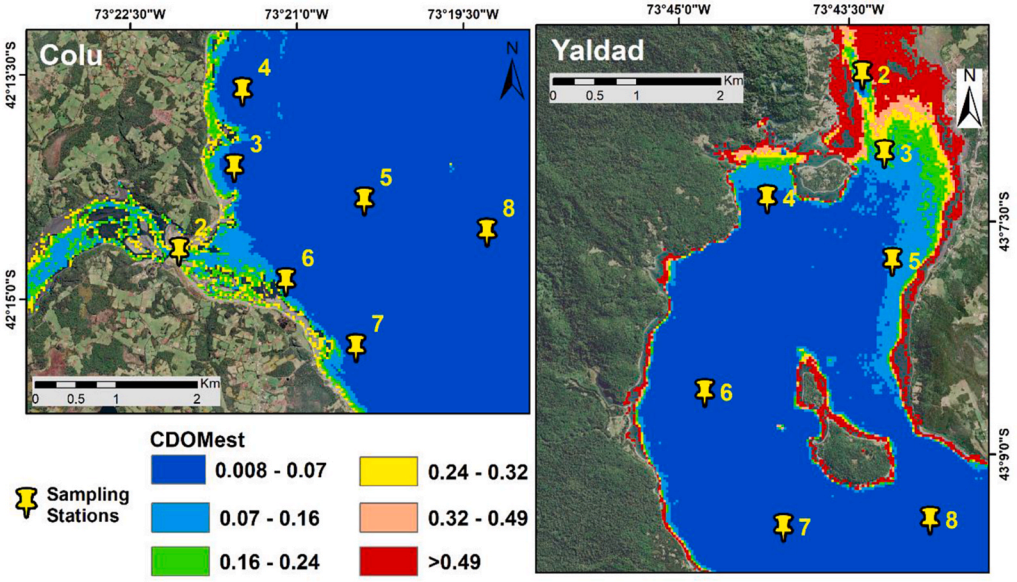

Fig. 3. Spatial distribution of CDOM*est* based on the Landsat 8 satellite images for the 2019 austral summer in the coastal areas of Colu and Yaldad Bay.

Colu area (Fig. 4; SM Table S12). The highest iPAR value, recorded in 2005, coincided with low CDOM*est* values in both study zones. Phytoplankton biomass, measured as Chl*a* and nFLH (SM Table S12) showed high values in Colu, whereas the values were significantly lower in Yaldad Bay, although in both areas the trend of Chl*a* remained relatively stable (Fig. 4).

Finally, as a conservative interpretation of association between variables, we consider a Spearman rank correlation (R_s), which is strong and significant when R_s => ±0.5 and $p \leq 0.05$ (Fig. 5). A positive and weak relationship between CDOM*est* and iPAR was observed (R_s = 0.18 and R_s = 0.33) in both zones respectively (Fig. 5a and b). In both zones (Fig. 5a, b), a significant correlation was observed between CDOM*est* and SST (R_s = −0.57 and R_s = −0.59; $p \leq 0.05$), respectively. A strong positive correlation nFLH-iPAR (R_s = 0.56; $p \leq 0.05$) and nFLH-SST (R_s = 0.50; $p \leq 0.05$) was also observed in Yaldad zone.

3.3. Land use change analysis

Our study watersheds had contrasting land uses (Fig. 6a), with the Colu river basin exhibiting a higher degree of human intervention. The dominant land use at Colu in 2020 corresponded to grassland-agriculture (35%) and shrublands (38%, Fig. 6b, SM Table S15a). The Yaldad river basin showed an opposite pattern during 2020, where the native forest dominated the landscape (82%, Fig. 6e, SM Table S15b). Land use change between 2000 and 2020 was significantly higher in the Colu watershed than in Yaldad – shrubland and grassland-agriculture areas increased by 14 and 10 km^2 respectively, whereas native forest coverage decreased by around 13 km^2 during this period (Fig. 6c; SM Table S15a). In the Yaldad watershed, both shrubland and native forest increased by 10 and 7 km^2, respectively, during the same period (Fig. 6f; SM Table S15b). It is worth noting that, in contrast to the Colu basin, we did not observe bare soil in the Yaldad basin.

As mentioned before, particular years (2007, 2013, 2014, 2016 and 2020) showed a different pattern of CDOM*est* (Fig. 4a, SM Table S12). This difference could be related to the land use of the watersheds. For this reason, land use changes were analyzed using five-year bins, i.e., 2000–2005, 2005–2010, 2010–2014 and 2014–2020. During 2000–2005, the shrublands in Colu watershed decreased by approximately 10 km^2 at a rate of change of −0.096 $km^2\ y^{-1}$, while grassland-agriculture increased by 9.35 km^2 at a rate of 0.081 km^2 per year (Table 2a; SM Table 16a). Similarly, we also observed an increase in grassland-agriculture of 8.34 km^2 with an annual rate of change of 0.078 $km^2\ y^{-1}$ between 2010 and 2014 (Table 2a; SM Table 16a). On the other hand, there was an evident decrease in the grassland-agriculture area of 5.3 and 5.9 km^2 for the periods 2005–2010 and 2014–2020, respectively. Finally, native forest cover in the Colu river basin evidenced a major decrease during the entire study period 2010–2014 and 2014–2020 (Table 2a) with an annual rate of change of −0.031 and 0.059 $km^2\ y^{-1}$, respectively (SM Table 16a).

The Yaldad watershed evidenced little significant changes in land use over time, which were only evident for native forest, shrubland and grasslands-agriculture (Table 2b). Native forest decreased during the 2000–2005 and 2014–2020 periods by 14.8 and 5.17 km^2, with an annual rate of change of −0.013 and −0.004 $km^2\ y^{-1}$, respectively. An increase of 17.3 km^2 (0.016 $km^2\ y^{-1}$) occurred during 2005–2010. Shrubland increased by 9.3 km^2 during 2000–2005, while a decrease of 12.1 km^2 was evident for the years 2005–2010. The annual rates of change were 0.063 and −0.081 $km^2\ y^{-1}$, for the 2000–2005 and 2005–2010 periods, respectively (SM Table S16b). The use of grassland-agriculture had a fluctuating behavior, in the periods 2000–2005 and 2014–2020, increasing 6.8 km^2 and 1.9 km^2, respectively (Table 2b). In the rest of the periods, 2005–2010 and 2010–2014 it decreased 6.4 km^2 and 1.16 km^2, respectively (Table 2b). The highest annual rate of change was in grassland-agriculture, with 0.136 and −0.110 $km^2\ y^{-1}$ during 2000–2005 and 2005–2010, respectively (SM Table S16b).

Fig. 7 shows the correlations of the CDOM*est* with the different land uses for each study zone. In the Colu zone (Fig. 7a), a strong positive correlation of CDOM*est* with urban (R_s = 0.53) and CDOM*est* with grassland (R_s = 0.56), which includes agricultural use was observed, whereas a negative correlation was observed between CDOM*est* and native forest (R_s = −0.75). On the other hand, the results evidenced how changing land uses interact; for instance, the strong negative correlation between grasslands and shrublands (R_s = −0.63), or as urban use increased, grasslands also increased (R_s = 0.76). In Yaldad Bay (Fig. 7b), we found a strong and positive correlation of CDOM*est* with urban uses (R_s = 0.59), wetland (R_s = 0.81) and native forest (R_s = 0.47), and a negative correlation of CDOM*est* with shrubland (R_s = −0.45) was observed. Conversely, there is a significant and negative correlation between native forest with shrubland R_s = −0.99; $p \leq 0.01$) and grassland-agriculture (R_s = −0.94).

Finally, a principal component analysis (PCA) for all years allowed us to examine the relationship among all the parameters in both study areas. The analysis highlighted the influence of land use as a driver of the spatial structure of the different parameters. The PCA showed three

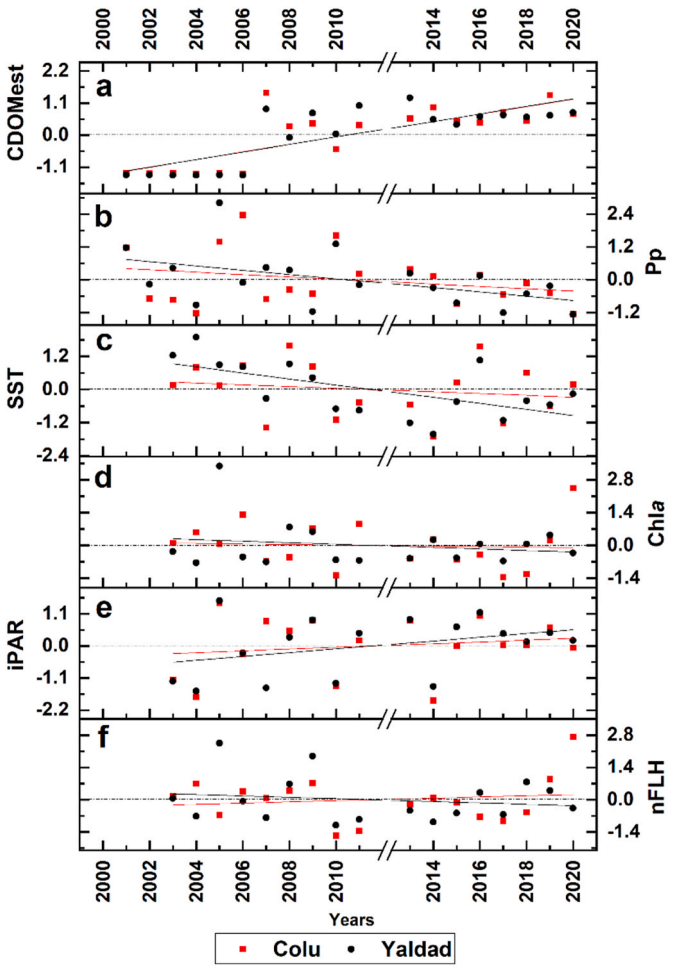

Fig. 4. Standardized anomalies for the 18-year temporal analysis in the Colu and Yaldad areas. The variables analyzed were: (a) CDOM*est* (m^{-1}), (b) precipitation (Pp; mm), (c) sea surface temperature (SST; °C), (d) chlorophyll-a (Chl*a*; mg m^{-3}), (e) instantaneous photosynthetically active radiation (iPAR; Einstein m^{-2} s^{-1}), (f) normalized fluorescence line height (nFLH - mW cm^{-2} μm^{-1} sr^{-1}). The red lines and squares correspond to the Colu zone, while the black lines and circles denote data for the Yaldad zone. We had no information for the years 2000 and 2012 because satellite images were too cloudy during the study period (austral summer). The environmental parameters SST, Chl*a*, iPAR and nFLH were estimated from MODIS-A imagery CDOM*est* estimates are based on Landsat 7 and 8, whereas precipitation data were obtained from weather stations of the region, available on the website www.CR2.cl. (For interpretation of the references to color in this figure legend, the reader is referred to the Web version of this article.)

principal components that jointly explained 79.5% of the total variance and the reduced dimensionality allowed a clear separation between the two watersheds (Fig. 8, SM Table S17). The first principal component (PC1) explained 57% of the interaction between variables; it was characterized by significant positive coefficients (weights >0.6) assigned to the variables CDOM*est,* Urban, Shrubland, Wetland, Native Forest, Water body (SM Table S17). A negative but significant coefficient was associated with SST, Chl*a* and Grassland (SM Table S17). The second principal component (PC2) accounted for 12% of the interaction, with a high but positive coefficient for nFLH (Fig. 8, SM Table S17). The third principal component (PC3), which explained 10%, clustered the variable iPAR with a high and positive coefficient (SM Table S17).

4. Discussion

4.1. Spectral slopes, indices, and the relationship of CDOM/fDOM to land use

The input of dissolved organic matter linked to anthropogenic disturbances plays an important role in the biogeochemistry of the coastal ocean (e.g., alterations in CO_2 flux, eutrophication, acidification) (Graeber et al., 2015; Regnier et al., 2013; Wilson and Xenopoulos, 2009). However, there are few reports (especially along the Chilean coast) on the influence of land uses and land use change on the availability of allochthonous chromophoric (CDOM) and fluorescent DOM (*f*DOM) (Curra-Sánchez et al., 2022; González et al., 2019; Nimptsch et al., 2015). The Colu and Yaldad rivers carried high concentration of CDOM to the coastal zone, which decreased as salinity increased (Fig. 3). Our observations agreed with other studies that showed that forest and vegetation types contribute to higher CDOM/*f*DOM availability in the river-ocean continuum (Sánchez-Pérez et al., 2020; Fierro et al., 2017; Williams et al., 2010). Furthermore, we found that fulvic and humic acid-like CDOM/*f*DOM dominate more aquatic ecosystems surrounded by forest, while agricultural and urban uses are more associated with protein-like compounds, tyrosine and humic acids (He et al., 2021; Fellman et al., 2010; Wilson and Xenopoulos, 2009; Stedmon et al., 2006).

Spectral slopes and the relationship between them are a potential indicator of the degradation, molecular weight, and origin of CDOM in aquatic environments (Valerio et al., 2018; Vantrepotte et al., 2015; Fichot and Benner, 2012; Helms et al., 2008). According to analyses of spectral slopes obtained *in situ*, the coastal zone of Colu was characterized by high values of S275–295 and S300-350, suggesting a decrease in aromaticity and molecular weight, consistent with increased photochemical degradation of terrestrial CDOM during its transport into the coastal ocean (Pandi et al., 2021; Guo et al., 2012; Helms et al., 2008). Exposure to solar radiation (Grunert et al., 2021; Zhang et al., 2009) also contributes to degradation and lower molecular weight of CDOM (Roiha et al., 2016; Fasching et al., 2014; Lapierre et al., 2013), and in our results an increase in iPAR radiation was observed for both study areas. In addition, a grassland-agricultural land use pattern could imply potential fertilizer and agrochemical inputs to the river and coastal zone (Williams et al., 2010; Stedmon et al., 2006). According to the literature (He et al., 2021; Roiha et al., 2016; Wilson and Xenopoulos, 2009) the development of agricultural activities and urban use contribute to CDOM that is less aromatic and more easily degraded by bacteria, which enhances bacterial abundance in adjacent aquatic ecosystems. Indeed, according to Curra-Sánchez et al. (2022), bacterial abundance was higher in the Colu River than in Yaldad River. Previous studies state that water residence or turnover time can influence dissolved organic matter degradation (e.g., photobleaching, microbial activity, etc.), transport, and permanence (Grunert et al., 2021; Kellerman et al., 2015; Kothawala et al., 2014; Shen and Wang, 2007). In our study areas, the average monthly water age is between 250 and 300 (coastal zone of Colu) and 50–80 (coastal zone of Yaldad Bay) days, respectively (according to the MIKE-3 model simulation of the ISC, www.chonos.ifop.cl), favoring protracted bacterial degradation processes. Similar results have been observed for other aquatic ecosystems, where land use influences the amount and type of CDOM, which in turn influences the community and abundance of bacteria that degrades CDOM (He et al., 2021; Roiha et al., 2016; Fasching et al., 2014; Wilson and Xenopoulos, 2009).

In Yaldad Bay the S275-295 is lower, *in situ* CDOM had a higher molecular weight and aromaticity (higher lignin, fulvic and humic acid content), and the watershed is less intervened by anthropogenic actions being dominated by native forest. This suggested that *in situ* CDOM was less degraded (Wagner et al., 2015; Fichot and Benner, 2012; Helms et al., 2008). Overall, this implies that allochthonous *in situ* CDOM could be mostly from forest materials (Garcia et al., 2018; Fellman et al., 2010; Williams et al., 2010; Helms et al., 2008). Our data are comparable with

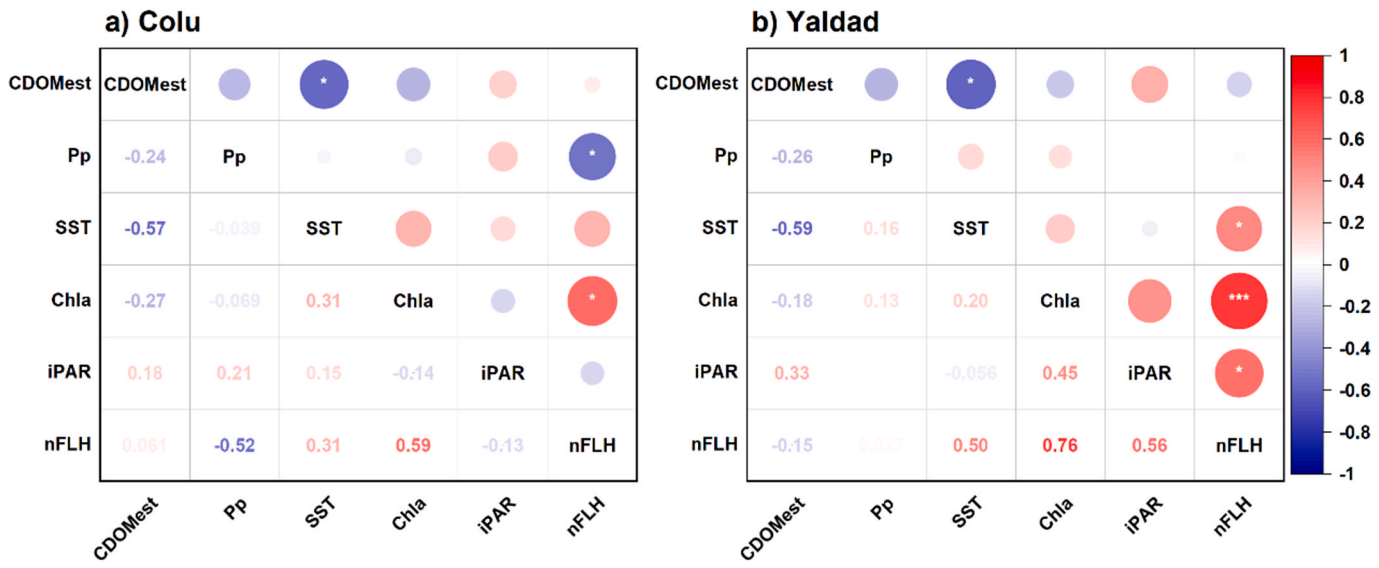

Fig. 5. Spearman correlation from the standardized temporal analysis of CDOM*est*, precipitation (Pp), sea surface temperature (SST), chlorophyll-a (Chl*a*), instantaneous photosynthetically active radiation (iPAR), and normalized fluorescence line height (nFLH) for (a) Colu and (b) Yaldad zone. The colors of the circles indicate the type of correlation, being positive (red) or negative (blue). The size and intensity of the color indicate the magnitude of the correlation. The white asterisk indicates the degree of significance of the correlation (*$p \leq 0.05$ **$p \leq 0.01$ ***$p \leq 0.001$). (For interpretation of the references to color in this figure legend, the reader is referred to the Web version of this article.)

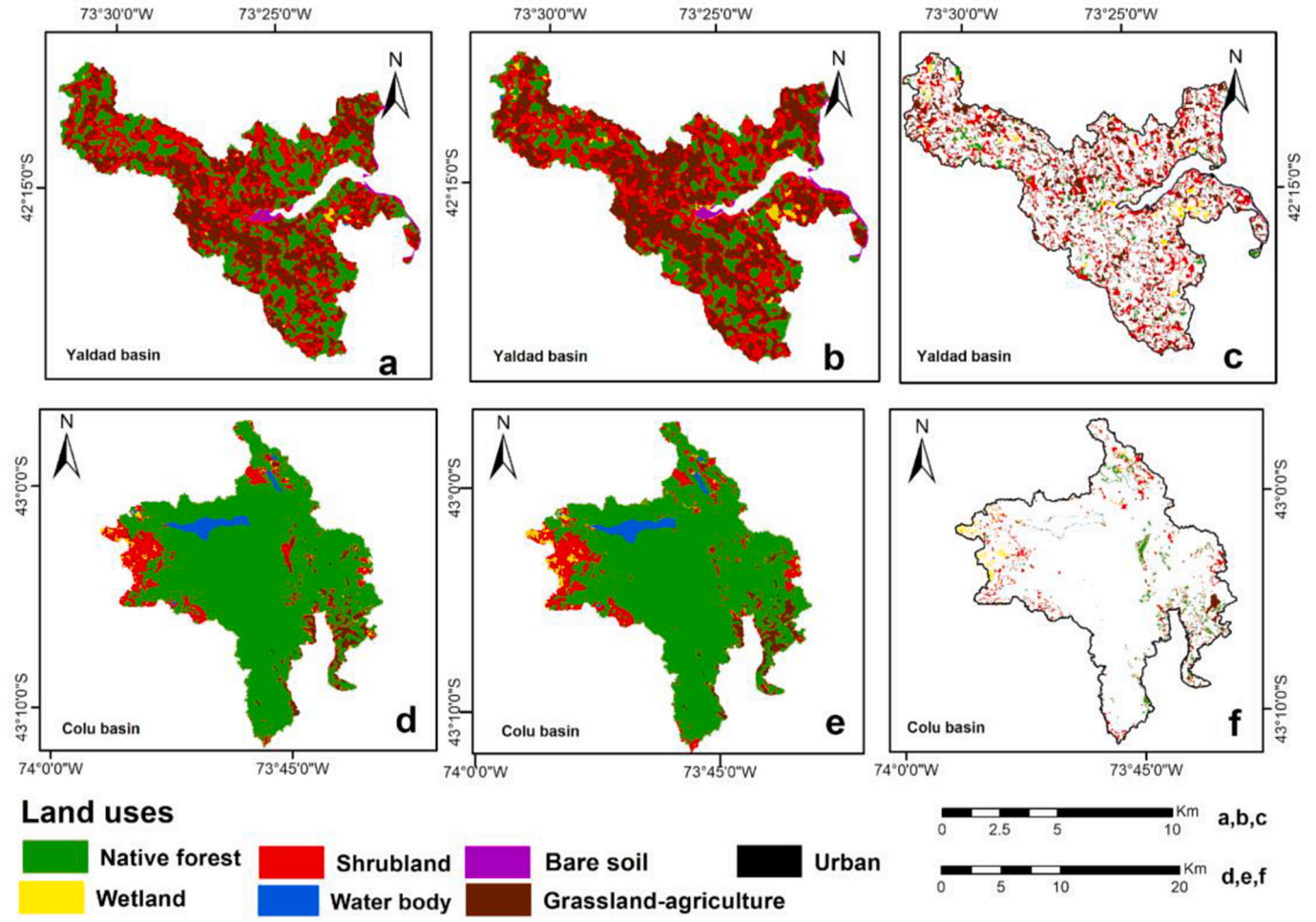

Fig. 6. Land use for the years 2000 (a, d) and 2020 (b, e) and the (c, f) change or difference symmetry of the (top panels) Colu River basin and (bottom panels) Yaldad River basin.

Table 2
Summary of land use data for (a) Colu and (b) Yaldad during the years 2000, 2005, 2010, 2014 and 2020 based on Landsat 7 and 8 satellite imagery.

(a) Land use Colu Basin from the year 2000–2020 Km^2										
Land use	2000	%	2005	%	2010	%	2014	%	2020	%
Native Forest	30.04	39.83	30.66	40.65	30.16	39.98	26.59	35.25	18.45	24.46
Shrubland	24.55	32.55	14.79	19.61	21.01	27.85	16.11	21.36	28.62	37.94
Wetland	0.32	0.42	0.32	0.42	0.30	0.40	0.24	0.32	1.16	1.54
Grassland-agriculture	19.62	26.01	28.97	38.41	23.64	31.34	31.98	42.40	26.12	34.63
Water body	0.03	0.04	0.03	0.04	0.03	0.04	0.03	0.04	0.03	0.04
Bare soil	0.87	1.15	0.59	0.78	0.22	0.29	0.41	0.54	0.98	1.30
Urban	0.00	0.00	0.07	0.09	0.07	0.09	0.07	0.09	0.07	0.09
Total	75.43	100	75.43	100	75.43	100	75.43	100	75.43	100
(b) Land use Yaldad Basin from the year 2000–2020 Km^2										
Land use	2000	%	2005	%	2010	%	2014	%	2020	%
Native Forest	226.53	83.83	211.71	78.35	228.99	84.75	227.66	84.25	222.49	82.34
Shrubland	26.12	9.67	35.40	13.10	23.22	8.59	25.91	9.59	28.58	10.58
Wetland	3.48	1.29	2.34	0.87	3.41	1.26	4.01	1.48	4.27	1.58
Grassland-agriculture	7.64	2.83	14.46	5.35	8.06	2.98	6.22	2.30	8.13	3.01
Water body	6.44	2.38	6.13	2.27	6.36	2.35	6.24	2.31	6.57	2.43
Urban	0.00	0.00	0.17	0.06	0.17	0.06	0.17	0.06	0.17	0.06
Total	270.21	100	270.21	100	270.21	100	270.21	100	270.21	100

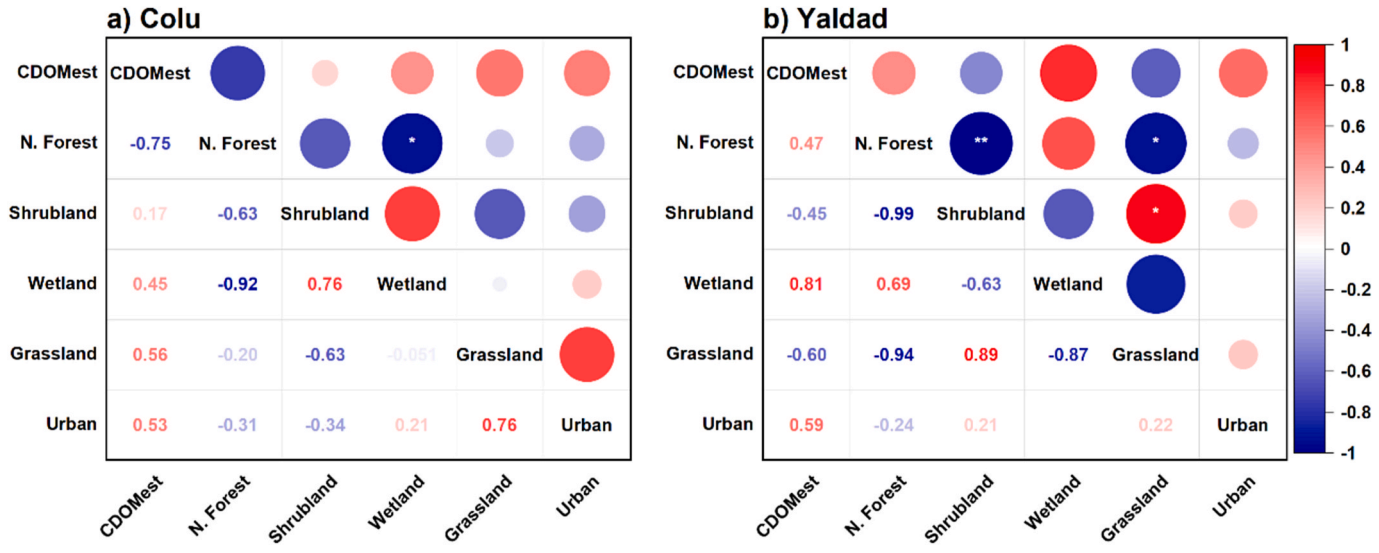

Fig. 7. Pearson correlation from standardized CDOM*est* from the temporal analysis and land use (Native forest - N. Forest, Shrubland, Wetland, Grassland-agriculture and Urban) for the years 2000, 2005, 2010, 2014 and 2020 for (a) Colu and (b) Yaldad. The color of the circles indicates the type of correlation, being positive (red) or negative (blue). The size and intensity of the color indicate the magnitude of the correlation. The white asterisk indicates the degree of significance of the correlation (*$p \leq 0.05$ **$p \leq 0.01$ ***$p \leq 0.001$). (For interpretation of the references to color in this figure legend, the reader is referred to the Web version of this article.)

other studies (Garcia et al., 2018; Fellman et al., 2010; Williams et al., 2010), where CDOM presented a more aromatic composition with humic and fulvic compounds (regions dominated by forest and wetlands). Therefore, we can infer that the degradation rate and exposure time of CDOM are lower in Yaldad Bay than the coastal area of Colu, according to the longer water residence time.

The fluorescence index (FI) and the humification index (HIX) have been used as a complement in studies of CDOM to distinguish different origins and the degree of CDOM transformation (Chen et al., 2011; Huguet et al., 2009). According to McKnight et al. (2001) and Cawley et al. (2012) the FI values tend to be lower in river samples and higher towards the open ocean, which coincides with our observations (Fig. 2, SM Table S7). The low FI values in the river samples indicate a fluorescence of terrestrial origin, and the higher FI combined with lower CDOM concentrations indicate a dilution of fluvial terrestrial CDOM with an increase in autochthonous CDOM of microbial origin from the marine zone (Shafiquzzaman et al., 2020; Cawley et al., 2012). In addition, high FI values suggest a predominance of materials derived from extracellular and leached release of bacteria and algae. These observations are consistent with those of McKnight et al. (2001), implying that microbially-derived fulvic acids have lower aromaticity and higher fluorescence indices than terrestrially derived fulvic acids observed in streams and rivers. In conclusion, the low values of spectral slopes (S275-295; S350-400; SR) and FI, together with high values of the HIX index observed in the Yaldad area corroborate that the predominant material is of terrestrial source with higher degree of humification and aromaticity (Fig. 2, SM Table S7).

Similar to the patterns observed by Chen et al. (2011) and Huguet et al. (2009), where HIX values decrease from rivers to bays, gulf and open ocean, our HIX values decreased from stations located in both rivers (maximum HIX: 9.04) to the marine zone (minimum HIX: 0.34) (Fig. 2, SM Table S7). This suggests that there would be more terrestrial

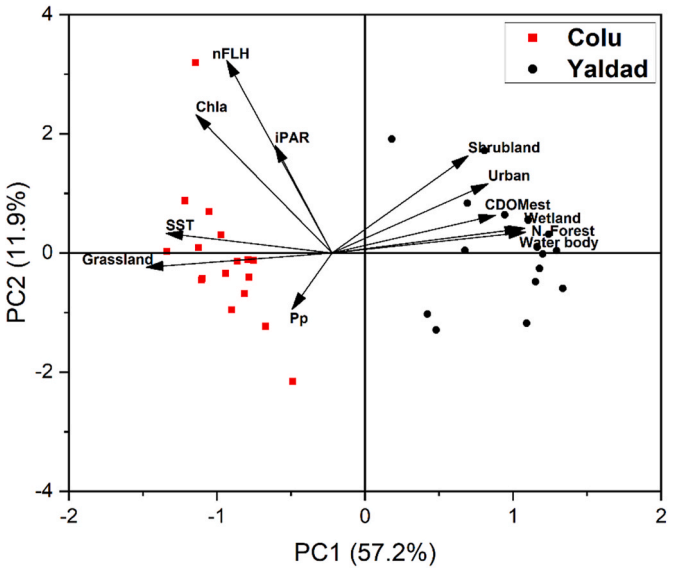

Fig. 8. Clustering based on Principal Component Analysis (PCA) of CDOM*est*, sea surface temperature (SST), precipitation (Pp), instantaneous photosynthetically active radiation (iPAR), chlorophyll-*a* (Chl*a*), normalized fluorescence line height (nFLH), and soil uses (Glassland, Urban, Shrubland, Wetland, Native Forest, Water body). The circles represent the study areas, Colu (red) and Yaldad (black). The axes correspond to the first two principal components (PC), which explain 69.1% of the total variance. (For interpretation of the references to color in this figure legend, the reader is referred to the Web version of this article.)

CDOM input in the rivers while microbially produced CDOM predominates in the bay and sea (Shang et al., 2019; Cawley et al., 2012; Shang et al., 2019). The differences in the values of the indices observed between the seasons of the campaigns (summer and austral spring) may be strongly influenced by the use and change of land use (Curra-Sánchez et al., 2022). The FI and HIX patterns agree with the results observed for spectral slopes (SM Table S7). These results provide background for our interpretation of the relationship between land use change and CDOM. For future work it would be interesting to address the decomposition of CDOM and its complex relationship with the autochthonous sources of aquatic DOM, microbial degradation and the contribution of phytoplankton. For example, Danhiez et al. (2017) demonstrate that the spectral slope between 320 nm and 412 nm can serve as a relevant indicator of the marine origin DOM, being related to phytoplankton bloom conditions.

4.2. Relationship of remote sensing of CDOM to land use in coastal regions

The water quality of aquatic ecosystems is degrading drastically as human activities increase along watersheds worldwide (Razali et al., 2018; Gholizadeh et al., 2016). Remote sensing techniques supported by traditional *in situ* sampling can provide comprehensive information with high spatial and temporal resolution, which can be leveraged as an economically and reliable monitoring strategy of water quality parameters such as CDOM (Drozdova et al., 2021; Valerio et al., 2021). The present study shows a simple and basic alternative to analyze the spatio-temporal pattern of CDOM*est* and the influence of land use change and relevant biophysical parameters in two small coastal areas comprising optically complex inland waters. Although *in situ* reflectance data would have been ideal, the coefficients obtained for our study areas (Table S6) and the *in situ* CDOM data proved to be a viable alternative for estimating CDOM (Fig. 3). It is well known that river inputs provide terrestrial dissolved organic matter to estuaries and coastal areas (Massicotte et al., 2017; Osburn et al., 2016). The improved statistical fit in austral spring would result from the pluvial regime that increases surface runoff to the coastal zone during winter and early spring in rivers of northern Patagonia (León-Muñoz et al., 2021; Pérez-Santos et al., 2021). The algorithms also allowed us to perform a calculation back in time to assess the temporal variations of CDOM*est* between both zones. In this way, after proper match-up assessment, the temporal analysis of CDOM*est* obtained a baseline study of CDOM dynamics in the aquatic ecosystem of these two remote and poorly studied areas of Northern Patagonia, Chile (Curra-Sánchez et al., 2022; González et al., 2019). Similarly, the analysis of CDOM*est* could also allow us to assess potential changes under future projections of climate change scenarios. For example, it has been shown that an increase in CDOM influences the parameters of the carbonate system (e.g., increasing pCO_2 – Valerio et al., 2018, and decreasing pH and carbonate saturation state) with negative effects on calcifying organisms (Curra-Sánchez et al., 2022; Vargas et al., 2017; Guo et al., 2012). Our results showed a significant correlation between land uses and CDOM*est*, suggesting that land use and land use change have a direct impact on the availability of coastal CDOM*est* over time and space. Previous research supports our finding; changes in land use influence the origin and quality of CDOM in aquatic ecosystems (He et al., 2021; Zhang et al., 2021; Fellman et al., 2010; Helms et al., 2008). While in the Colu watershed grassland-agriculture and urban uses showed the highest correlation and influence with CDOM*est* (Fig. 7a), native forest and urban use were positively correlated with CDOM*est* in Yaldad (Fig. 7b), supporting the hypothesis that each dominant use influenced the CDOM*est* observed in the water of each coastal zone. The findings of González et al. (2019) at the ISC support the above, observing that the contribution of humic substances was enhanced along the fjord-ocean transect by inputs from intense forestry and agricultural activity around the Puelo River basin. Whereas Curra-Sánchez et al. (2022) observed in the river-ocean continuum of the Yaldad basin high values of the humic acid component (UVA and UVC) and terrestrial fulvic acids resulting from the contribution of native forest.

The PCA analysis illustrated the influence of environmental variables in each zone, highlighting a relationship with land use. For example, the role of native forest, wetland and shrubland cover was evident in the concentration of CDOM*est* in the Yaldad area and its divergence with pasture (agriculture) and the rest of the environmental variables in the Colu area (Fig. 8). In this study we demonstrated a rising trend in the CDOM*est* (Fig. 4) in both study areas, with values showing an initial increase in 2007, measuring 0.194 and 0.807 m^{-1} in Colu and Yaldad, respectively. This variation in the CDOM*est* was influenced by land use changes. According to Curra-Sánchez et al. (2022) land use influences *in situ* CDOM availability in the adjacent coastal zones. CDOM*est* was lower in the Colu zone where the predominant area of the contributing watershed is covered by grassland-agriculture (34%), whereas the availability of *in situ* CDOM was higher and the predominant area of the watershed was occupied by native forest (80%) in Yaldad. The years 2005, 2007 and 2008, when the CDOM*est* values were higher in Colu than in Yaldad, coincided with periods of land cover change where the area of grassland-agriculture increased. Because of this change, the soil was washed, and a higher content of dissolved organic matter was dragged to the water bodies. Alvarez-Garreton et al. (2019) and Salas et al. (2016), reported that the area of native forest throughout Chile decreased between 250000 to about 3 million ha. in the last 35 years (1974–2016), because of land use change (e.g., forest plantations and agro-industrial activities, mainly). Following the results from our area and elsewhere (Curra-Sánchez et al., 2022; Williams et al., 2010), land use and land use change patterns over time are posited to alter the quantity and quality of CDOM exported by forests and wetlands into rivers and coastal areas.

4.3. Environmental factors influencing CDOM in the coastal zone

Satellite-derived nFLH and Chl*a* are used in the literature as proxies

for biomass or productivity phytoplankton, due to the limited availability of *in situ* data in northern Patagonia (Jacques-Coper et al., 2023; Saldías and Lara, 2020; Lara et al., 2016). High values of Chl*a* and nFLH were found in Colu (northern part of the ISC), whereas lower values characterized Yaldad (Fig. 4). Our temporal patterns are comparable with other studies (Vásquez et al., 2021; Saldías et al., 2019, 2021; Lara et al., 2016) showing a seasonal pattern and elevated Chl*a* values indicating a high phytoplankton biomass in the northern Patagonian region (north of Desertores Islands) as compared to the southern ISC where Yaldad Bay is located. However, our results of CDOM*est* for the past 18 years are the first attempt to understand past variability as there is no temporal information to empirically compare the study areas (2001–2011 and 2013 to 2020).

Our results of the coastal regions could also be greatly influenced by the local oceanographic conditions north and south of Desertores Island and their seasonal variability (León-Muñoz et al., 2021; Pérez-Santos et al., 2021; Lara et al., 2016). The water age or residence time is higher (200–400 days) north of Desertores Island and lower (50–200 days) in the southern ISC, which is conditioned by wind circulation and water stratification (Pinilla et al., 2020). During austral fall and winter, westerlies are stronger, and the mixing of the surface layer increases, while during spring-summer, the westerly flow weakens, increasing the stratification and decreasing the water age (Pérez-Santos et al., 2021; Saldías et al., 2019; Lara et al., 2016). Therefore, this suggests that degradation processes act for a longer time on the available CDOM in the coastal zone around Colu. On the other hand, the bacterial abundance is also higher in the Colu River than in Yaldad (Curra-Sánchez et al., 2022), and thus, bacterial degradation would be also higher in this zone, which is also supported by the higher FI index in Colu (Table S8). Primary productivity contributes to autochthonous CDOM, which is corroborated by high Chl*a* values. In our study high chlorophyll values only coincided with high CDOM*est* values in the Colu coastal zone, suggesting that part of CDOM composition has an autochthonous origin derived from phytoplankton (González et al., 2019; Zhang et al., 2013). According to different authors (e.g., Vásquez et al., 2021; González et al., 2019; Lara et al., 2010, 2016), the region north of Desertores Island (coastal zone of Colu) presents high chlorophyll concentrations during austral spring-summer and fall compared with the southern ISC (Yaldad Bay). These local oceanographic conditions should be influencing the residence, transport, and degradation of CDOM over time and space. The study of CDOM should be considered for the monitoring and planning of mussel farming activity in these coastal regions and in other similar zones around the world. This work represents the first attempt to use satellite data for a CDOM estimation in northern Patagonia, Chile. Considering that there is no data of CDOM (for such a long period) in Chilean waters, neither *in situ* nor estimated, this study represents a major step towards increasing our understanding of water quality dynamics nearshore.

5. Conclusions

Our results demonstrate the need to continue the study of land-ocean interactions, which are not only affected by climate change but also by the intense development of anthropogenic activity (e.g., land cover change). This study showed that land use and land use change are the main factors influencing the availability of CDOM*est*. Empirical associations showed that predominant land use in the watershed has a significant relationship with the CDOM*est* that reaches the coastal zone. CDOM*est* showed contrasting relationships between watersheds with the amount of native forest cover. In general, we can conclude that grassland-agriculture use altered the quantity and quality of the CDOM*est* compared to that exported by the native forest to the rivers and coastal ocean. Moreover, oceanographic conditions along the Inner Sea of Chiloé played a key role in the variability of CDOM*est* and should be considered in greater detail in future works. The spectral slopes and the FI and HIX indices corroborate that the Yaldad area is dominated by CDOM of terrestrial origin with a high degree of aromaticity and humification, the result of the predominant use of native forest. In contrast, less aromatic and more degraded material of microbial origin would be associated with predominant agricultural, and livestock use in Colu. The increasing trend of CDOM availability in both study areas may have implications for biogeochemical cycles, with implications for aquaculture in the coastal region. *In situ* and estimated CDOM values at the river station were higher than the values observed at the rest of the coastal stations. Regression analyses showed that the inclusion of the CDOM values measured at the river's stations had a strong influence on the relationships between *in situ* CDOM and CDOM*est* for both zones and seasons. Finally, our results suggest that including other oceanographic and climatic parameters, in addition to land use change, would help to better understand the CDOM dynamics and the causes of its variations in the coastal region.

Funding sources

This study was funded by National Agency for Research and Development of Chilean Government (Program BECAS-ANID) – 21170394 grant and (Program FONDECYT- POSTDOCTORAL-ANID) – 3240540 grant ECS and by ANID through Fondo Nacional de Desarrollo Científico y Tecnológico (FONDECYT) grant 1230420 to CL, 1130132 to JN, 1220167 to GSS, 1221699 to BRB, 1210171 to CAV. AdMV was funded by São Paulo Research Foundation (FAPESP, 2018/18491-4, 2020/08148-0). Additional support was provided by ANID – Millennium Science Initiative Program SECOS - ICN2019_015, Millennium Science Initiative Nucleus UPWELL - NCN19-153, Fondo de Investigación Estratégica en Sequía - ANID FSEQ210030, and COPAS Coastal ANID FB210021. W.G was funded by Fundación Data Observatory, Centro Tecnológico ANID DO210001.

Open research

Data Availability Statement: Landsat images were retrieved from the online Data Pool, courtesy of the NASA Land Processes Distributed ActiveArchive Center (LP DAAC), USGS/EarthResources (https://earthexplorer.usgs.gov/accessed on January 11, 2021) Observation and Science (EROS) Center, SiouxFalls, South Dakota (https://lpdaac.usgs.gov/products/mod13q1v006/accessed on January 11, 2021).Wind data are available at Physical Oceanography Distributed Active Archive Center (PODAAC) website (https://podaac.jpl.nasa.gov/accessed on October 18, 2021). SST, Chl*a*, iPAr and data are available at NASA's Ocean color website (http://oceancolor.gsfc.nasa.gov accessed on October 18, 2021). Precipitation data are available at Centro de Investigación del Clima y la Resiliencia (CR2). Explorador Climático, website (www.cr2.cl, www.explorador.cr2.cl accessed on September 10, 2021). The water permanence time data were obtained from Chonos is an oceanographic information system resulting from environmental studies designed for the development of numerical modeling in Chilean Patagonia. Departamento de Medio Ambiente, División de Acuicultura del Instituto de Fomento Pesquero (IFOP) website (www.chonos.ifop.cl accessed on December 27, 2021). **All the data used for the research are in the supplementary material, a copy of which will also be provided in CSV format.**

CRediT authorship contribution statement

Elizabeth D. Curra-Sánchez: Writing – review & editing, Writing – original draft, Visualization, Validation, Resources, Methodology, Investigation, Formal analysis, Data curation, Conceptualization. **Aline de M. Valerio:** Writing – review & editing, Validation, Supervision, Methodology, Formal analysis, Conceptualization. **Carlos Lara:** Writing – review & editing, Visualization, Supervision, Methodology, Conceptualization. **Wirmer García-Tuñon:** Writing – review & editing, Visualization, Validation, Methodology, Investigation, Data curation,

Conceptualization. **Bernardo R. Broitman:** Writing – review & editing, Supervision, Methodology, Data curation, Conceptualization. **Gonzalo S. Saldías:** Writing – review & editing, Visualization, Supervision, Methodology, Data curation. **Jorge Nimptsch:** Writing – review & editing, Validation, Methodology, Data curation. **Cristian A. Vargas:** Writing – review & editing, Supervision, Investigation, Conceptualization.

Declaration of competing interest

The authors declare that they have no known competing financial interests or personal relationships that could have appeared to influence the work reported in this paper.

Data availability

Data will be made available on request.

Acknowledgments

We are acknowledged by the Coastal Ecosystems & Global Environmental Change Lab" (ECCA Lab) for their valuable help and support during sampling and laboratory analysis. Also acknowledged by the National Agency for Research and Development of Chilean Government (Program FONDECYT- POSTDOCTORAL-ANID) – 3240540. The authors would like to thank Sebastian Osorio for laboratory support of Laboratorio de Bioensayos y Limnología Aplicada, Instituto de Ciencias Marinas y Limnológicas UACh, Universidad Austral de Chile for infrastructure used for CDOM and *f*DOM analysis. We acknowledges by the Núcleo de Investigación en Data Science (NIDS), Facultad de Ingeniería y Negocios, Universidad de las Américas, Santiago, Chile for support.

Appendix A. Supplementary data

Supplementary data to this article can be found online at https://doi.org/10.1016/j.ecss.2024.108897.

References

Aguayo, M., Pauchard, A., Azócar, G., Parra, O., 2009. Cambio del uso del suelo en el centro sur de Chile a fines del siglo XX: Entendiendo la dinámica espacial y temporal del paisaje. Rev. Chil. Hist. Nat. 82 (3), 361–374. https://doi.org/10.4067/S0716-078X2009000300004.

Alvarez-Garreton, C., Lara, A., Boisier, J.P., Galleguillos, M., 2019. The impacts of native forests and forest plantations on water supply in Chile. Forests 10 (6), 473. https://doi.org/10.3390/F10060473. Vol. 10, Page 473.

APHA, 2005. Standard Methods for the Examination of Water and Wastewater, twenty-first ed. American Public Health Association, American Water Works Association, Water Environment Federation, Washington DC, USA, p. 940 https://www.standardmethods.org/doi/book/10.2105/SMWW.2882.

Behrenfeld, M.J., Westberry, T.K., Boss, E.S., O'Malley, R.T., Siegel, D.A., Wiggert, J.D., Franz, B.A., McClain, C.R., Feldman, G.C., Doney, S.C., Moore, J.K., Dall'Olmo, G., Milligan, A.J., Lima, I., Mahowald, N., 2009. Satellite-detected fluorescence reveals global physiology of ocean phytoplankton. Biogeosciences 6 (5), 779–794. https://doi.org/10.5194/BG-6-779-2009.

Biblioteca del Congreso Nacional de Chile. (n.d.). Biblioteca del Congreso Nacional de Chile - BCN. Territorial information of Chile, Mapoteca. Retrieved January 14, 2020, from https://www.bcn.cl/portal.

Boyd, P.W., Lennartz, S.T., Glover, D.M., Doney, S.C., 2015. Biological ramifications of climate-change-mediated oceanic multi-stressors. Nat. Clim. Change 2014 5 (1), 71–79. https://doi.org/10.1038/nclimate2441.

Bricaud, A., Morel, A., Prieur, L., 1981. Absorption by dissolved organic matter of the sea (yellow substance) in the UV and visible domains1. Limnol. Oceanogr. 26 (1), 43–53. https://doi.org/10.4319/LO.1981.26.1.0043.

Cawley, K.M., Butler, K.D., Aiken, G.R., Larsen, L.G., Huntington, T.G., McKnight, D.M., 2012. Identifying fluorescent pulp mill effluent in the Gulf of Maine and its watershed. Mar. Pollut. Bull. 64 (8), 1678–1687. https://doi.org/10.1016/J.MARPOLBUL.2012.05.040.

Chen, C., He, X., Liu, Z., Sun, W., Dong, H., Chu, Y., 2020. Analysis of regional economic development based on land use and land cover change information derived from Landsat imagery. Scientific Reports 2020 10 (1), 1–16. https://doi.org/10.1038/s41598-020-69716-2, 1, 10.

Chen, H., Zheng, B., Song, Y., Qin, Y., 2011. Correlation between molecular absorption spectral slope ratios and fluorescence humification indices in characterizing CDOM. Aquat. Sci. 73 (1), 103–112. https://doi.org/10.1007/S00027-010-0164-5/METRICS.

Chen, J., Zhu, W.N., Tian, Y.Q., Yu, Q., 2017. Estimation of colored dissolved organic matter from landsat-8 imagery for complex inland water: case study of lake huron. IEEE Trans. Geosci. Rem. Sens. 55 (4), 2201–2212. https://doi.org/10.1109/TGRS.2016.2638828.

Chen, M., Li, C., Spencer, R.G.M., Maie, N., Hur, J., McKenna, A.M., Yan, F., 2021. Climatic, land cover, and anthropogenic controls on dissolved organic matter quantity and quality from major alpine rivers across the Himalayan-Tibetan Plateau. Sci. Total Environ. 754 https://doi.org/10.1016/J.SCITOTENV.2020.142411.

Chuvieco, E., 2010. Teledetección ambiental: La observación de la Tierra desde el espacio. Editorial Ariel Colección Ariel Ciencia Nueva, p. 592.

Clasing, E., Brey, T., Stead, R., Navarro, J., Asencio, G., 1994. Population dynamics of Venus antiqua (Bivalvia: Veneracea) in the Bahía de Yaldad, Isla de Chiloé, Southern Chile. J. Exp. Mar. Biol. Ecol. 177 (2), 171–186. https://doi.org/10.1016/0022-0981(94)90235-6.

Coble, P.G., Del Castillo, C.E., Avril, B., 1998. Distribution and optical properties of CDOM in the arabian sea during the 1995 southwest monsoon. Deep Sea Res. Part II Top. Stud. Oceanogr. 45 (10–11), 2195–2223. https://doi.org/10.1016/S0967-0645(98)00068-X.

Coble, P.G., 2007. Marine optical biogeochemistry: the chemistry of Ocean Color. Chem. Rev. 107 (2), 402–418. https://doi.org/10.1021/cr050350+.

Congedo, L., 2021. Semi-Automatic Classification Plugin: a Python tool for the download and processing of remote sensing images in QGIS. J. Open Source Softw. 6 (64), 3172. https://doi.org/10.21105/JOSS.03172.

Corporación Nacional Forestal - Conaf/Universidad Austral de Chile - Uach, 2014. INFORME FINAL "Monitoreo de cambios, corrección cartográfica y actualización del catastro de recursos Vegetacionales Nativos de la Región de Los Lagos. http://sit.conaf.cl.

Curra-Sánchez, E.D., Lara, C., Cornejo-D'Ottone, M., Nimptsch, J., Aguayo, M., Broitman, B.R., Saldías, G.S., Vargas, C.A., 2022. Contrasting land-uses in two small river basins impact the colored dissolved organic matter concentration and carbonate system along a river-coastal ocean continuum. Sci. Total Environ. 806, 150435 https://doi.org/10.1016/J.SCITOTENV.2021.150435.

Danhiez, P., Vantrepotte, V., Cauvin, A., Lebourg, E., Loisel, H., 2017. Optical properties of chromophoric dissolved organic matter during a phytoplankton bloom. Implication for DOC estimates from CDOM absorption. Limnol. Oceanogr. 62 (4), 1409–1425. https://doi.org/10.1002/lno.10507.

del Castillo, C.E., Miller, R.L., 2008. On the use of ocean color remote sensing to measure the transport of dissolved organic carbon by the Mississippi River Plume. Rem. Sens. Environ. 112 (3), 836–844. https://doi.org/10.1016/J.RSE.2007.06.015.

Dirección General de Aguas. (n.d.). Dirección General de Aguas (DGA) Chilean Ministry of Public Works. Hydro-meteorological information. Retrieved March 10, 2021, from https://dga.mop.gob.cl/Paginas/default.aspx.

Drozdova, A.N., Nedospasov, A.A., Lobus, N.v., Patsaeva, S.v., Shchuka, S.A., 2021. CDOM optical properties and DOC content in the largest mixing zones of the siberian shelf seas. Rem. Sens. 13, 1145. https://doi.org/10.3390/RS13061145, 13(6)2021, 1145.

D'Sa, E.J., Miller, R.L., 2003. Bio-optical properties in waters influenced by the Mississippi River during low flow conditions. Rem. Sens. Environ. 84 (4), 538–549. https://doi.org/10.1016/S0034-4257(02)00163-3.

FAO, 1996. Forest Resources Assessment 1990. Survey of Tropical Forest Cover and Study of Change Processes.

FAO, 2020. The state of world fisheries and aquaculture 2020. In: Sustainability in Action, vol. 244. The State of World Fisheries and Aquaculture. https://doi.org/10.4060/CA9231EN, 2020.

Fasching, C., Behounek, B., Singer, G.A., Battin, T.J., 2014. Microbial degradation of terrigenous dissolved organic matter and potential consequences for carbon cycling in brown-water streams. Scientific Reports 2014 4 (1), 1–7. https://doi.org/10.1038/srep04981, 4:1,.

Fellman, J.B., Hood, E., Spencer, R.G.M., 2010. Fluorescence spectroscopy opens new windows into dissolved organic matter dynamics in freshwater ecosystems: a review. Limnol. Oceanogr. 55 (6), 2452–2462. https://doi.org/10.4319/LO.2010.55.6.2452.

Ficek, D., Zapadka, T., Dera, J., 2011. Remote sensing reflectance of Pomeranian lakes and the Baltic. Oceanologia 53 (4), 959–970. https://doi.org/10.5697/OC.53-4.959.

Fichot, C.G., Benner, R., 2012. The spectral slope coefficient of chromophoric dissolved organic matter (S275–295) as a tracer of terrigenous dissolved organic carbon in river-influenced ocean margins. Limnol. Oceanogr. 57 (5), 1453–1466. https://doi.org/10.4319/LO.2012.57.5.1453.

Fierro, P., Bertrán, C., Tapia, J., Hauenstein, E., Peña-Cortés, F., Vergara, C., Cerna, C., Vargas-Chacoff, L., 2017. Effects of local land-use on riparian vegetation, water quality, and the functional organization of macroinvertebrate assemblages. Sci. Total Environ. 609, 724–734. https://doi.org/10.1016/J.SCITOTENV.2017.07.197.

Garcia, R.D., Diéguez, M. del C., Gerea, M., Garcia, P.E., Reissig, M., 2018. Characterisation and reactivity continuum of dissolved organic matter in forested headwater catchments of Andean Patagonia. Freshw. Biol. 63 (9), 1049–1062. https://doi.org/10.1111/FWB.13114.

Gholizadeh, M.H., Melesse, A.M., Reddi, L., 2016. A comprehensive review on water quality parameters estimation using remote sensing techniques. Sensors 16, 1298. https://doi.org/10.3390/S16081298, 16(8), 1298 2016.

González, H.E., Nimptsch, J., Giesecke, R., Silva, N., 2019. Organic matter distribution, composition and its possible fate in the Chilean North-Patagonian estuarine system. Sci. Total Environ. 657, 1419–1431. https://doi.org/10.1016/J.SCITOTENV.2018.11.445.

Graeber, D., Boëchat, I.G., Encina-Montoya, F., Esse, C., Gelbrecht, J., Goyenola, G., Gücker, B., Heinz, M., Kronvang, B., Meerhoff, M., Nimptsch, J., Pusch, M.T., Silva, R.C.S., Von Schiller, D., Zwirnmann, E., 2015. Global effects of agriculture on fluvial dissolved organic matter. Sci. Rep. 5 (1), 1–8. https://doi.org/10.1038/srep16328, 2015 5:1.

Grunert, B.K., Tzortziou, M., Neale, P., Menendez, A., Hernes, P., 2021. DOM degradation by light and microbes along the Yukon River-coastal ocean continuum. Sci. Rep. 11 (1), 1–14. https://doi.org/10.1038/s41598-021-89327-9, 2021 11:1.

Guo, W., Yang, L., Yu, X., Zhai, W., Hong, H., 2012. Photo-production of dissolved inorganic carbon from dissolved organic matter in contrasting coastal waters in the southwestern Taiwan Strait, China. J. Environ. Sci. (China) 24 (7), 1181–1188. https://doi.org/10.1016/S1001-0742(11)60921-2.

Hao, S., Zhu, F., Cui, Y., 2021. Land use and land cover change detection and spatial distribution on the Tibetan Plateau. Scientific Reports 2021 11 (1), 1–13. https://doi.org/10.1038/s41598-021-87215-w, 11:1,.

He, Q., Gao, L., Wang, Z., Tang, Y., Pan, B., Li, M., 2021. Fluorescence characteristics of dissolved organic matter in several independent water bodies: possible sources and land-use effects. Environ. Sci. Pollu. Res. 2021 28 (25), 33241–33253. https://doi.org/10.1007/S11356-021-12972-0, 28:25.

Helms, J.R., Stubbins, A., Ritchie, J.D., Minor, E.C., Kieber, D.J., Mopper, K., 2008. Absorption spectral slopes and slope ratios as indicators of molecular weight, source, and photobleaching of chromophoric dissolved organic matter. Limnol. Oceanogr. 53 (3), 955–969. https://doi.org/10.4319/LO.2008.53.3.0955.

Hu, B., Wang, P., Qian, J., Wang, C., Zhang, N., Cui, X., 2017. Characteristics, sources, and photobleaching of chromophoric dissolved organic matter (CDOM) in large and shallow Hongze Lake, China. J. Great Lake. Res. 43 (6), 1165–1172. https://doi.org/10.1016/J.JGLR.2017.09.004.

Huguet, A., Vacher, L., Relexans, S., Saubusse, S., Froidefond, J.M., Parlanti, E., 2009. Properties of fluorescent dissolved organic matter in the Gironde Estuary. Org. Geochem. 40 (6), 706–719. https://doi.org/10.1016/J.ORGGEOCHEM.2009.03.002.

Jacques-Coper, M., Segura, C., de la Torre, M.B., Valdebenito Muñoz, P., Vásquez, S.I., Narváez, D.A., 2023. Synoptic-to-intraseasonal atmospheric modulation of phytoplankton biomass in the inner sea of Chiloé, Northwest Patagonia (42.5°-43.5°S, 72.5°-74°W), Chile. Front. Mar. Sci. 10, 1160230 https://doi.org/10.3389/fmars.2023.1160230.

Kellerman, A.M., Kothawala, D.N., Dittmar, T., Tranvik, L.J., 2015. Persistence of dissolved organic matter in lakes related to its molecular characteristics. Nat. Geosci. 8 (6), 454–457. https://doi.org/10.1038/ngeo2440, 2014 8:6,.

Kothawala, D.N., Stedmon, C.A., Müller, R.A., Weyhenmeyer, G.A., Köhler, S.J., Tranvik, L.J., 2014. Controls of dissolved organic matter quality: evidence from a large-scale boreal lake survey. Global Change Biol. 20 (4), 1101–1114. https://doi.org/10.1111/GCB.12488.

Kutser, T., Verpoorter, C., Paavel, B., Tranvik, L.J., 2015. Estimating lake carbon fractions from remote sensing data. Rem. Sens. Environ. 157, 138–146. https://doi.org/10.1016/J.RSE.2014.05.020.

Lambert, T., Bouillon, S., Darchambeau, F., Morana, C., Roland, F.A.E., Descy, J.P., Borges, A.V., 2017. Effects of human land use on the terrestrial and aquatic sources of fluvial organic matter in a temperate river basin (The Meuse River, Belgium). Biogeochemistry 136 (2), 191–211. https://doi.org/10.1007/S10533-017-0387-9/FIGURES/9.

Lapierre, J.F., Guillemette, F., Berggren, M., del Giorgio, P.A., 2013. Increases in terrestrially derived carbon stimulate organic carbon processing and CO2 emissions in boreal aquatic ecosystems. Nat. Commun. 4 (1), 1–7. https://doi.org/10.1038/ncomms3972, 2013 4:1.

Lara, C., Miranda, M., Montecino, V., Iriarte, J.L., 2010. Chlorophyll-a MODIS mesoscale variability in the Inner Sea of Chiloé, Patagonia, Chile (41-43°S): patches and gradients? Rev. Biol. Mar. Oceanogr. 45 (2), 217–225. https://doi.org/10.4067/S0718-19572010000200003.

Lara, C., Saldías, G.S., Paredes, A.L., Cazelles, B., Broitman, B.R., 2018. Temporal variability of MODIS phenological indices in the temperate rainforest of northern Patagonia. Rem. Sens. 10 (6), 956. https://doi.org/10.3390/RS10060956, 2018, Vol. 10, Page 956.

Lara, C., Saldías, G.S., Tapia, F.J., Iriarte, J.L., Broitman, B.R., 2016. Interannual variability in temporal patterns of Chlorophyll–a and their potential influence on the supply of mussel larvae to inner waters in northern Patagonia (41–44°S). J. Mar. Syst. 155, 11–18. https://doi.org/10.1016/J.JMARSYS.2015.10.010.

Lawaetz, A., Stedmon, C., 2009. Fluorescence intensity calibration using the Raman scatter peak of water. Appl. Spectrosc. 63, 936–940. https://doi.org/10.1366/000370209788964548.

León-Muñoz, J., Aguayo, R., Marcé, R., Catalán, N., Woelfl, S., Nimptsch, J., Arismendi, I., Contreras, C., Soto, D., Miranda, A., 2021. Climate and land cover trends affecting freshwater inputs to a fjord in northwestern Patagonia. Front. Mar. Sci. 8, 960. https://doi.org/10.3389/FMARS.2021.628454/BIBTEX.

Mannino, A., Novak, M.G., Hooker, S.B., Hyde, K., Aurin, D., 2014. Algorithm development and validation of CDOM properties for estuarine and continental shelf waters along the northeastern U.S. coast. Rem. Sens. Environ. 152, 576–602. https://doi.org/10.1016/J.RSE.2014.06.027.

Massicotte, P., Asmala, E., Stedmon, C., Markager, S., 2017. Global distribution of dissolved organic matter along the aquatic continuum: across rivers, lakes and oceans. Sci. Total Environ. 609, 180–191. https://doi.org/10.1016/J.SCITOTENV.2017.07.076.

McKnight, D.M., Boyer, E.W., Westerhoff, P.K., Doran, P.T., Kulbe, T., Andersen, D.T., 2001. Spectrofluorometric characterization of dissolved organic matter for indication of precursor organic material and aromaticity. Limnol. Oceanogr. 46 (1), 38–48. https://doi.org/10.4319/LO.2001.46.1.0038.

Miller, J.N., 1981. Correction of excitation and emission spectra. Standards in Fluorescence Spectrometry. Springer, Dordrecht, pp. 49–67. https://doi.org/10.1007/978-94-009-5902-6_7.

Nelson, N.B., Siegel, D.A., 2013. The global distribution and dynamics of chromophoric dissolved organic matter. Ann. Rev. Mar. Sci 5, 447–476. https://doi.org/10.1146/ANNUREV-MARINE-120710-100751.

Nezlin, N.P., Beegan, C., Feit, A., Gully, J.R., Latker, A., McLaughlin, K., Mengel, M.J., Robertson, G.L., Steele, A., Weisberg, S.B., 2020. Colored Dissolved Organic Matter (CDOM) as a tracer of effluent plumes in the coastal ocean. Reg. Stud. Mar. Sci. 35, 101163 https://doi.org/10.1016/J.RSMA.2020.101163.

Nimptsch, J., Woelfl, S., Kronvang, B., Giesecke, R., González, H.E., Caputo, L., Gelbrecht, J., von Tuempling, W., Graeber, D., 2014. Does filter type and pore size influence spectroscopic analysis of freshwater chromophoric DOM composition? Limnologica 48, 57–64. https://doi.org/10.1016/J.LIMNO.2014.06.003.

Nimptsch, J., Woelfl, S., Osorio, S., Valenzuela, J., Ebersbach, P., von Tuempling, W., Palma, R., Encina, F., Figueroa, D., Kamjunke, N., Graeber, D., 2015. Tracing dissolved organic matter (DOM) from land-based aquaculture systems in North Patagonian streams. Sci. Total Environ. 537, 129–138. https://doi.org/10.1016/J.SCITOTENV.2015.07.160.

Ogallo, L., Gbeckor-Kove, N., 1989. *Climate Variations Drought and Desertification. Report of the CCL Repporteur on Drought and Desertification in Warm Climates to the Tenth Session of the Commision for Climatology* (W.-No. 286 World Climate Programme/WCAP-7. World Meteorological Organization (WMO). https://library.wmo.int/index.php?lvl=notice_display&id=11547#.YeM4kP7MLrc.

Osburn, C.L., Boyd, T.J., Montgomery, M.T., Bianchi, T.S., Coffin, R.B., Paerl, H.W., 2016. Optical proxies for terrestrial dissolved organic matter in estuaries and coastal waters. Front. Mar. Sci. 2 (JAN), 127. https://doi.org/10.3389/fmars.2015.00127.

Pandi, S.R., Chari, N.V.H.K., Sarma, N.S., Chiranjeevulu, G., Kiran, R., Murthy, K.N., Venkatesh, P., Lotliker, A.A., Tripathy, S.C., 2021. Characteristics of conservative and non-conservative CDOM of a tropical monsoonal estuary in relation to changing biogeochemistry. Reg. Stud. Mar. Sci. 44, 101721 https://doi.org/10.1016/J.RSMA.2021.101721.

Pérez, C.A., DeGrandpre, M.D., Lagos, N.A., Saldías, G.S., Cascales, E.K., Vargas, C.A., 2015. Influence of climate and land use in carbon biogeochemistry in lower reaches of rivers in central southern Chile: implications for the carbonate system in river-influenced rocky shore environments. J. Geophys. Res.: Biogeosciences 120 (4), 673–692. https://doi.org/10.1002/2014JG002699.

Pérez-Santos, I., Díaz, P.A., Silva, N., Garreaud, R., Montero, P., Henríquez-Castillo, C., Barrera, F., Linford, P., Amaya, C., Contreras, S., Aracena, C., Pinilla, E., Altamirano, R., Vallejos, L., Pavez, J., Maulen, J., 2021. Oceanography time series reveals annual asynchrony input between oceanic and estuarine waters in Patagonian fjords. Sci. Total Environ. 798, 149241 https://doi.org/10.1016/J.SCITOTENV.2021.149241.

Pinilla, E., Soto, G., Soto-Riquelme, C., Venegas, O., Salas, P., Cortés, J., Moya, M., Vergara, M., 2020. Determinación de las Escalas de Intercambio de Agua en Fiordos y Canales de la Región de los Lagos y Región de Aysén del General Carlos Ibáñez del Campo. http://biblioteca.ifop.cl/exlibris/aleph/u23_1/adam_objects/ifp01/view/4/000037095.pdf.

Razali, A., Syed Ismail, S.N., Awang, S., Praveena, S.M., Zainal Abidin, E., 2018. Land use change in highland area and its impact on river water quality: a review of case studies in Malaysia. Ecol. Process. 7 (1), 1–17. https://doi.org/10.1186/S13717-018-0126-8/TABLES/7.

Regnier, P., Friedlingstein, P., Ciais, P., Mackenzie, F.T., Gruber, N., Janssens, I.A., Laruelle, G.G., Lauerwald, R., Luyssaert, S., Andersson, A.J., Arndt, S., Arnosti, C., Borges, A.V., Dale, A.W., Gallego-Sala, A., Goddéris, Y., Goossens, N., Hartmann, J., Heinze, C., et al., 2013. Anthropogenic perturbation of the carbon fluxes from land to ocean. Nat. Geosci. 6 (8), 597–607. https://doi.org/10.1038/ngeo1830, 2013 6:8.

Roiha, T., Peura, S., Cusson, M., Rautio, M., 2016. Allochthonous carbon is a major regulator to bacterial growth and community composition in subarctic freshwaters. Sci. Rep. 2016 6 (1), 1–12. https://doi.org/10.1038/srep34456, 6:1.

Romera-Castillo, C., Álvarez-Salgado, X.A., Galí, M., Gasol, J.M., Marrasé, C., 2013. Combined effect of light exposure and microbial activity on distinct dissolved organic matter pools. A seasonal field study in an oligotrophic coastal system (Blanes Bay, NW Mediterranean). Mar. Chem. 148, 44–51. https://doi.org/10.1016/j.marchem.2012.10.004.

Salas, C., Donoso, P.J., Vargas, R., Arriagada, C.A., Pedraza, R., Soto, D.P., 2016. The forest sector in Chile: an overview and current challenges. J. For. 114 (5), 562–571. https://doi.org/10.5849/JOF.14-062.

Saldías, G.S., Hernández, W., Lara, C., Muñoz, R., Rojas, C., Vásquez, S., Pérez-Santos, I., Soto-Mardones, L., 2021. Seasonal variability of SST fronts in the Inner Sea of Chiloé and its adjacent coastal ocean, northern Patagonia. Rem. Sens. 13 (2), 181. https://doi.org/10.3390/RS13020181, 2021, Vol. 13, Page 181.

Saldías, G.S., Lara, C., 2020. Satellite-derived sea surface temperature fronts in a river-influenced coastal upwelling area off central–southern Chile. Reg. Stud. Mar. Sci. 37, 101322 https://doi.org/10.1016/J.RSMA.2020.101322.

Saldías, G.S., Sobarzo, M., Quiñones, R., 2019. Freshwater structure and its seasonal variability off western Patagonia. Prog. Oceanogr. 174, 143–153. https://doi.org/10.1016/J.POCEAN.2018.10.014.

Sánchez-Pérez, E.D., Pujo-Pay, M., Ortega-Retuerta, E., Conan, P., Peters, F., Marrasé, C., 2020. Mismatched dynamics of dissolved organic carbon and chromophoric dissolved organic matter in the coastal NW Mediterranean Sea. Sci. Total Environ. 746, 141190 https://doi.org/10.1016/J.SCITOTENV.2020.141190.

SERNAPESCA - Servicio Nacional de Pesca y Acuicultura, 2018. *Anuario Estadístico de Pesca, 2018.* Ministerio de Economía, Fomento y Turismo. http://www.sernapesca.cl/.

Shafiquzzaman, M., Haider, H., Bhuiyan, M.A., Ahmed, A.T., AlSaleem, S.S., Ghumman, A.R., 2020. Spatiotemporal variations of DOM components in the Kushiro River impacted by a wetland. Environ. Sci. Pollut. Control Ser. 27 (15), 18287–18302. https://doi.org/10.1007/S11356-020-08192-7/METRICS.

Shang, Y., Song, K., Jacinthe, P.A., Wen, Z., Lyu, L., Fang, C., Liu, G., 2019. Characterization of CDOM in reservoirs and its linkage to trophic status assessment across China using spectroscopic analysis. J. Hydrol. 576, 1–11. https://doi.org/10.1016/J.JHYDROL.2019.06.028.

Shao, T., Wang, T., 2020. Effects of land use on the characteristics and composition of fluvial chromophoric dissolved organic matter (CDOM) in the Yiluo River watershed, China. Ecol. Indicat. 114, 106332 https://doi.org/10.1016/J.ECOLIND.2020.106332.

Shen, J., Wang, H.V., 2007. Determining the age of water and long-term transport timescale of the Chesapeake Bay. Estuar. Coast Shelf Sci. 74 (4), 585–598. https://doi.org/10.1016/J.ECSS.2007.05.017.

Silva, N., Vargas, C.A., Prego, R., 2011. Land–ocean distribution of allochthonous organic matter in surface sediments of the Chiloé and Aysén interior seas (Chilean Northern Patagonia). Continent. Shelf Res. 31 (3–4), 330–339. https://doi.org/10.1016/J.CSR.2010.09.009.

Slonecker, E.T., Jones, D.K., Pellerin, B.A., 2016. The new Landsat 8 potential for remote sensing of colored dissolved organic matter (CDOM). Mar. Pollut. Bull. 107 (2), 518–527. https://doi.org/10.1016/J.MARPOLBUL.2016.02.076.

Stedmon, C.A., Markager, S., Søndergaard, M., Vang, T., Laubel, A., Borch, N.H., Windelin, A., 2006. Dissolved organic matter (DOM) export to a temperate estuary: seasonal variations and implications of land use. Estuar. Coast 29 (3), 388–400. https://doi.org/10.1007/BF02784988, 2006 29:3.

Stedmon, C.A., Bro, R., 2008. Characterizing dissolved organic matter fluorescence with Parallel factor analysis: a tutorial. Limnol Oceanogr. Methods 6, 572–579. https://doi.org/10.4319/LOM.2008.6.572.

Subiabre, A., Rojas, C., 1994. *Geografía Física de la Región de Los Lagos* (Publicación N°4, p. 118). Ediciones Universidad Austral de Chile. Dirección de Investigación y Desarrollo.

Tiwari, S.P., Shanmugam, P., 2011. An optical model for the remote sensing of coloured dissolved organic matter in coastal/ocean waters. Estuar. Coast Shelf Sci. 93 (4), 396–402. https://doi.org/10.1016/J.ECSS.2011.05.010.

USGS Earth Explorer. (n.d.). Data set images of Landsat 8 Collection Level-1. Retrieved January 15, 2020, from https://earthexplorer.usgs.gov/.

Valerio, A., Kampel, M., Vantrepotte, V., Ward, N.D., Richey, J.E., 2021. Optical classification of lower amazon waters based on *in situ* data and sentinel-3 ocean and land color instrument imagery. Rem. Sens. 13 (16), 3057. https://doi.org/10.1364/OE.26.00A657, 2021, Vol. 13, Page 3057.

Valerio, A., Kampel, M., Vantrepotte, V., Ward, N.D., Richey, J.E., 2018. Using CDOM optical properties for estimating DOC concentrations and pCO2 in the Lower Amazon River. Opt Express 26 (14), 21. https://doi.org/10.1364/OE.26.00A657.

Vantrepotte, V., Danhiez, F.-P., Loisel, H., Ouillon, S., Mériaux, X., Cauvin, A., Dessailly, D., 2015. CDOM-DOC relationship in contrasted coastal waters: implication for DOC retrieval from ocean color remote sensing observation. Opt Express 23 (1), 33. https://doi.org/10.1364/OE.23.000033.

Vargas, C.A., Lagos, N.A., Lardies, M.A., Duarte, C., Manríquez, P.H., Aguilera, V.M., Broitman, B., Widdicombe, S., Dupont, S., 2017. Species-specific responses to ocean acidification should account for local adaptation and adaptive plasticity. Nat. Ecol. Evol. 1 (4), 1–7. https://doi.org/10.1038/s41559-017-0084, 2017 1:4,.

Vásquez, S.I., Belén De La Torre, M., Saldías, G.S., Montecinos, A., Lausch, A., Bumberger, J., Oppelt, N., 2021. Meridional changes in satellite chlorophyll and fluorescence in optically-complex coastal waters of northern Patagonia. Rem. Sens. 13 (5), 1026. https://doi.org/10.3390/RS13051026, 2021, Vol. 13, Page 1026.

Wagner, S., Jaffé, R., Cawley, K., Dittmar, T., Stubbins, A., 2015. Associations between the molecular and optical properties of dissolved organic matter in the Florida Everglades, a model coastal wetland system. Front. Chem. 3 (NOV), 66. https://doi.org/10.3389/FCHEM.2015.00066/BIBTEX.

Wang, X., Zhang, F., 2018. Effects of land use/cover on surface water pollution based on remote sensing and 3D-EEM fluorescence data in the Jinghe Oasis. Sci. Rep. 2018 8 (1), 1–13. https://doi.org/10.1038/s41598-018-31265-0, 8:1.

Ward, N.D., Bianchi, T.S., Medeiros, P.M., Seidel, M., Richey, J.E., Keil, R.G., Sawakuchi, H.O., 2017. Where carbon goes when water flows: carbon cycling across the aquatic continuum. Front. Mar. Sci. 4, 7. https://doi.org/10.3389/FMARS.2017.00007/BIBTEX.

Williams, C.J., Yamashita, Y., Wilson, H.F., Jaffe, R., Xenopoulos, M.A., 2010. Unraveling the role of land use and microbial activity in shaping dissolved organic matter characteristics in stream ecosystems. Limnol. Oceanogr. 55 (3), 1159–1171. https://doi.org/10.4319/LO.2010.55.3.1159.

Wilson, H.F., Xenopoulos, M.A., 2009. Effects of agricultural land use on the composition of fluvial dissolved organic matter. Nat. Geosci. 2 (1), 37–41. https://doi.org/10.1038/ngeo391, 2009 2:1.

Zhang, Y., Liu, M., Qin, B., Feng, S., 2009. Photochemical degradation of chromophoric-dissolved organic matter exposed to simulated UV-B and natural solar radiation. Hydrobiologia 627 (1), 159–168. https://doi.org/10.1007/S10750-009-9722-Z, 2009 627:1.

Zhang, Y., Liu, X., Wang, M., Qin, B., 2013. Compositional differences of chromophoric dissolved organic matter derived from phytoplankton and macrophytes. Org. Geochem. 55, 26–37. https://doi.org/10.1016/J.ORGGEOCHEM.2012.11.007.

Zhang, Y., Zhou, L., Zhou, Y., Zhang, L., Yao, X., Shi, K., Jeppesen, E., Yu, Q., Zhu, W., 2021. Chromophoric dissolved organic matter in inland waters: present knowledge and future challenges. Sci. Total Environ. 759, 143550 https://doi.org/10.1016/J.SCITOTENV.2020.143550.

Zhao, J., Cao, W., Xu, Z., Ai, B., Yang, Y., Jin, G., Wang, G., Zhou, W., Chen, Y., Chen, H., Sun, Z., 2018. Estimating CDOM concentration in highly turbid estuarine coastal waters. J. Geophys. Res.: Oceans 123 (8), 5856–5873. https://doi.org/10.1029/2018JC013756.